GEODYNAMICAL STUDIES IN THE NEAR EAST MEDITERRANEAN AND RED SEA REGION USING GPS AND SEISMOLOGICAL DATA ANALYSIS

By

***H. Khalil, **M. Becker, *Abdel-Monem S.M, *K, Sakr, *S. Mahmoud, *H. Hussain, Abou El Einen, *Ali K. Abdel-Fattah, ***A. Al Aydros and *Aly Rayan**

The Research work deals with Kinematics and Dynamics of the active areas in the Near East Mediterranean and Red Sea regions and extends to the Southern part of the Red Sea to include the major territories of Yemen. The prototype of the Red Sea as a classical continental rifting is focused to show its spreading. The collaborative effort is extended to use Global Positioning System (GPS) observations to measure directly the present-day style and rates of extension and rift-margin deformation along the extent of the Red Sea rift and the northern part of Africa versus Europe mainly, the Near East

* National Research Institute of Astronomy and Geophysics, Helwan, Cairo, Egypt.
** Institute of Geodesy, UBW, Munich.
*** Faculty of Science, Sanaa University.

Mediterranean. The field observations comprise measurements of GPS campaigns, Apr., 2000, Oct., 2001 and Dec., 2003, through a geodetic networks in Egypt and Yemen beside the IGS permanent stations around the study regions. We used GPS constraints on present-day deformation with available seismological data analysis for understanding and threw lights upon the geodynamical regime of the study regions.

Introduction

The subject of the research is dealing with the use of GPS and seismological data for the investigation of recent crustal kinematics for geodynamical studies on the seismo-active areas in the Near East Mediterranean and Red Sea regions.

The seismological data were used for processing the focal mechanism solutions as a combined solution. Bernese V.4.2 Software was used, among other facilities of the available GPS and seismological data in the area.

The independence of Recent Crustal Movements Laboratory (NRIAG in Egypt) has introduced in the last few years the technology of the Global Positioning System (GPS) for observing and detecting the crustal deformations in the seismo-active areas in Egypt through the geodetic networks, e.g. Sinai, Red Sea, Middle of Upper Egypt and around Nasser Lake at Aswan. Thus, the plan of study has been developed for global measurements through the international cooperation between NRIAG and Sana'a University through an established GPS geodetic network includes some geodetic points in Yemen and another in Egypt. Three GPS campaigns between Egypt and Yemen were measured in Apr., 2000, Oct., 2001 and Dec., 2003 respectively. The analysis processes of GPS and the seismological data played a great role for understanding and threw lights upon the geodynamical regime of the area and to evaluate a general framework of the study regions.

Applied Techniques

A) GPS Measurements

For the evaluation of the observed Yemen-Egypt GPS geodetic network in 2000, 2001 and 2003; a combination from selected IGS stations was set up with five sites in Yemen and five sites in Egypt. Figure (1) shows the IGS sites WTZR, MATE, RAMO, AMMN, BAHR, IISC and MALI which were analyzed through the observed campaigns. The IGS sites serve as anchor stations to tie the regional network to the International Terrestrial Reference Frame ITRF 2000. Figure (1) includes also the configuration of the GPS geodetic network Yemen-Egypt. Figure (2) shows the sites of some established geodetic points in Yemen.

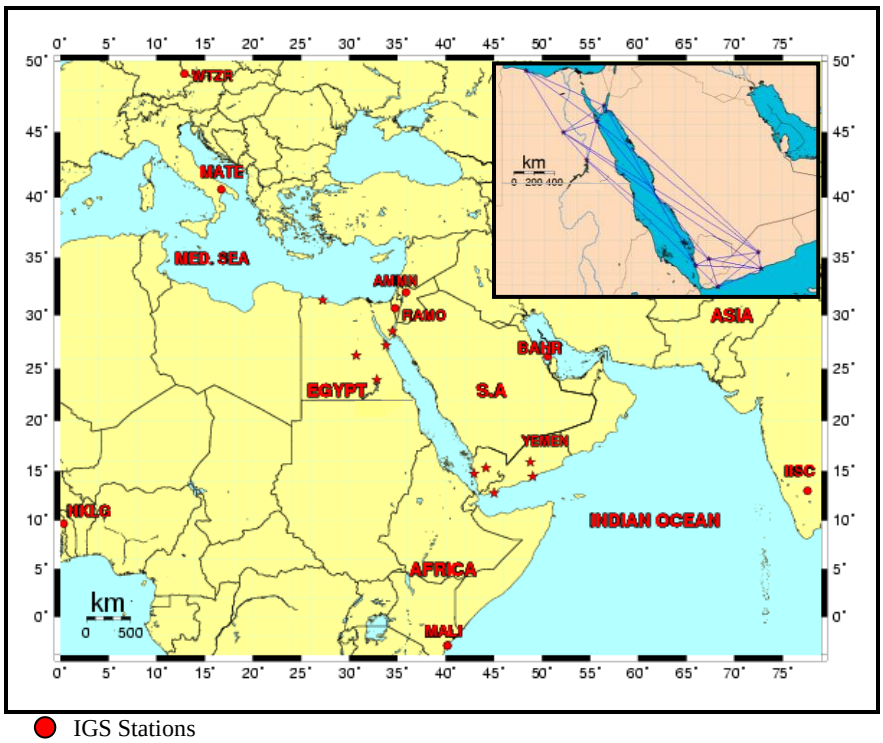

IGS Stations
GPS Geodetic Points in both Egypt and Yemen

Fig. (1) : Shows the points of Egypt-Yemen GPS Geodetic Network.

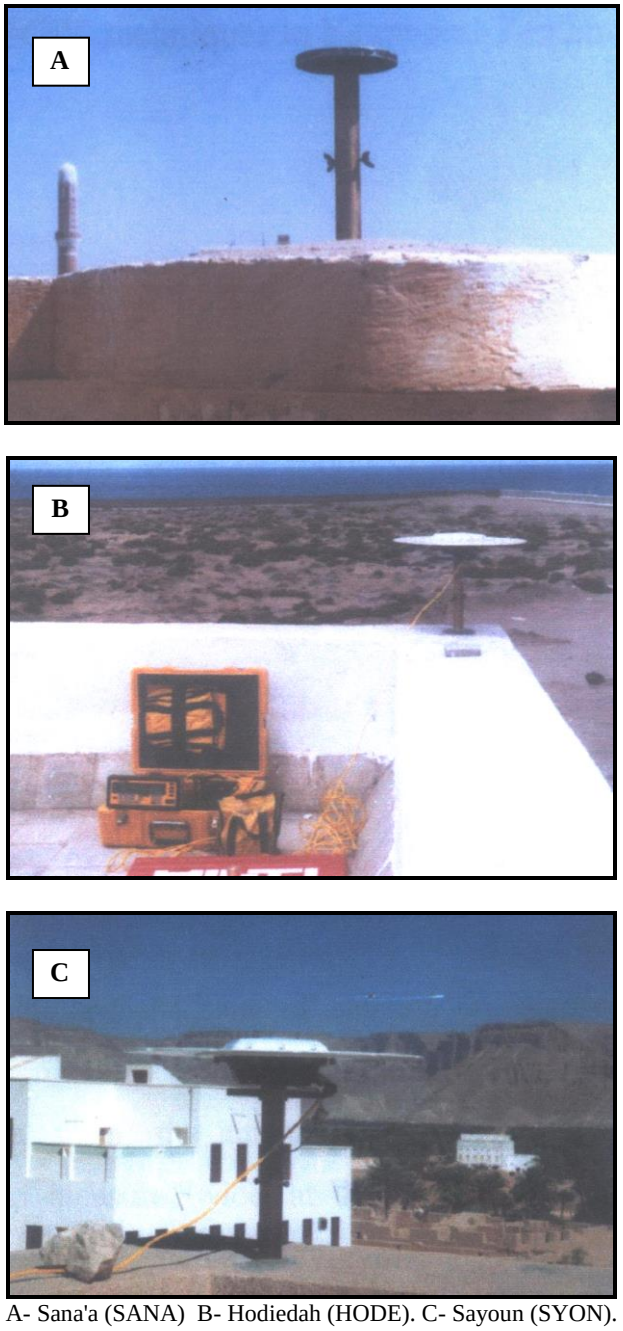

A- Sana'a (SANA) B- Hodiedah (HODE). C- Sayoun (SYON).

Fig. (2): Shows the Locations of some GPS stations in Yemen.

Using of this combination not only the deformation within the network could be detected but also the motion components in the ITRF 2000 directly are obtained. The three campaigns were evaluated following the standards for high quality reference frame GPS works as described (Matthias, 2002). Results of an Ionosphere-free L3 solution are derived from all sessions in each epoch and saved as an epoch solution. The loose solutions of each epoch were combined and constraint by the motions of the IGS anchor sites in the ITRF 2000 reference frame.

GPS and other new techniques are used to study ground deformation associated with earthquakes. Our study focuses on combining GPS data from a geodetic network and focal mechanisms deduced from the seismological data analysis considering some previous studies which were carried out in the study region beside the analysis and interpretation which carried out by our team. The dealing of GPS Data analysis will be portrayed after the discussion of the seismological data analysis

B) Focal Mechanism

It is well known that most earthquake occurrences are due to a sudden rupture taking place along faults in the earth. Some of these faults have a surface rupture associated with the earthquake. As most of the fault ruptures of earthquakes do not reach the earth surface and is thus not directly visible. Seismological approaches such as the focal mechanism study are indispensable for studying seismic faults and their rupture process, the focal mechanism bears information not only on seismic faults, but also on the tectonics around the earthquake source region, plate motion and the tectonic stress which causes the earthquake. Plate motions on the earth surface are now inferred from slip vectors of fault plane solutions obtained for a large number of earthquakes over the world. The seismic fault model of earthquakes is based on the analysis of seismic waves.

i. Seismicity and Focal Mechanisms of the Near East African Margin

The earthquake activity of this margin is related to shelf and continental slope extending from the shelf break down to the Nile cone. It is more or less parallel to the Egyptian shore. It extends from Cyrenaica (Eastern Libya) to the northern part of Sinai. Some authors (Sofratome Group, 1984; Ben-Avraham et al., 1987) indicated that the continental margin can be considered as a weakness zone having experienced thinning during the Triassic period. This transition zone between the faulted continental and oceanic crusts might be predestined in N110°-120°E orientation and to be reactivated with dextral strike slip and reverse fault component. Figure (3) shows the relative seismic activities in the northern part of the study region. This part is diffuse and do not constitute any lineaments which may be restricted to the accuracy of data specially for this part because it is far from both Egyptian stations and European stations. A cluster of the seismic activity is clearly shown along the northeastern part of Libya (Cyrenaica) which represent the closest area to the subduction process beneath Hellenic arc. Few larger events are located along the Egyptian coastal shelf. The focal mechanisms of larger events along this margin reflect a transition from a tensional stress to the south of the continental shelf to compressional stress to the south of the subduction zone (Fig. 4).

ii. Seismicity and Focal Mechanisms of the Hellenic Arc:

The shallow earthquake activity (h<60 km) is contained in a belt parallel to the Hellenic and Cyprean arcs (Fig. 3). The rate of activity is higher in the Hellenic arc than in the Cyprean arc. The activity of the Hellenic arc extends from Albania in the West to Eastern Turkey in the East. The activity is mostly seaward of the islands and all large events occur between the deepest part of the trench and islands. Few shocks lie as far as the Mediterranean ridge and the swell south of the deep basins.

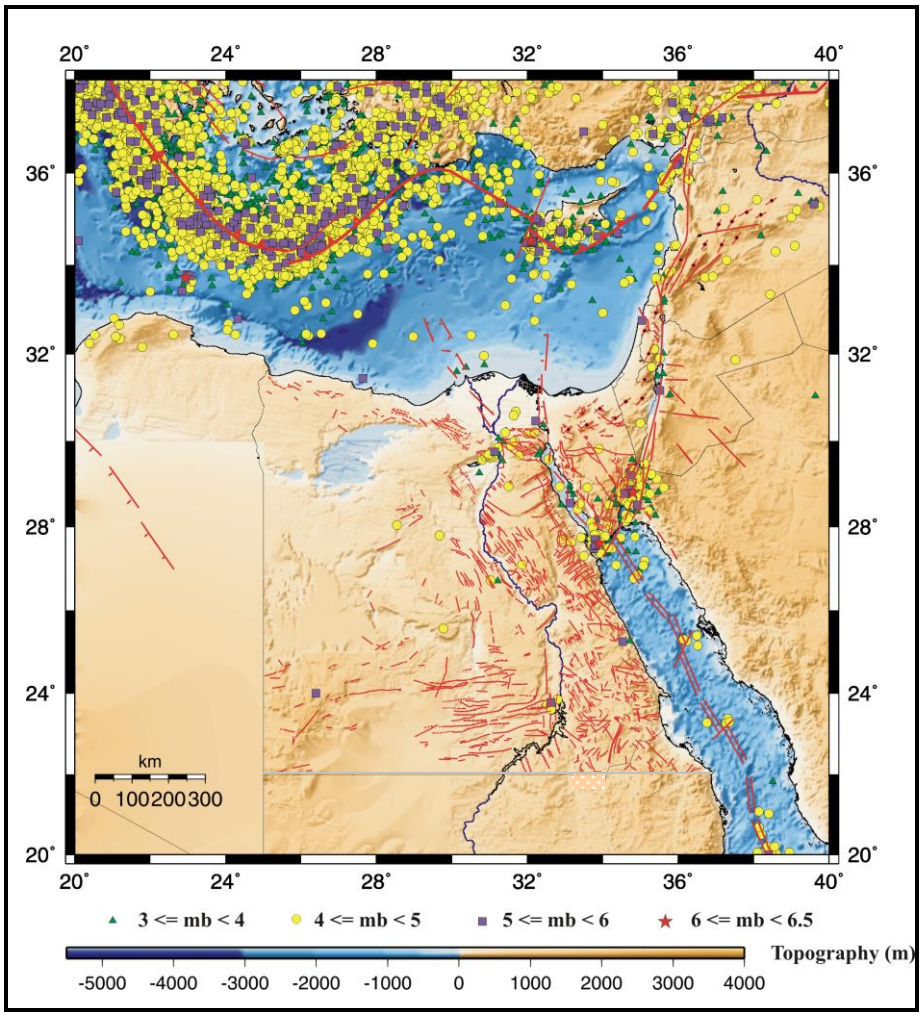

Fig. (3): Seismicity map of the East Mediterranean Regionn from 1964-2003 (ISC) Data. and Regional tectonic setting. A compiled map from Sofratome Group (1984), Abou Elenean (1997), Reilinger et al., (2000), Egyptian Geological Survey (1981) and Salamon et al., (1996).

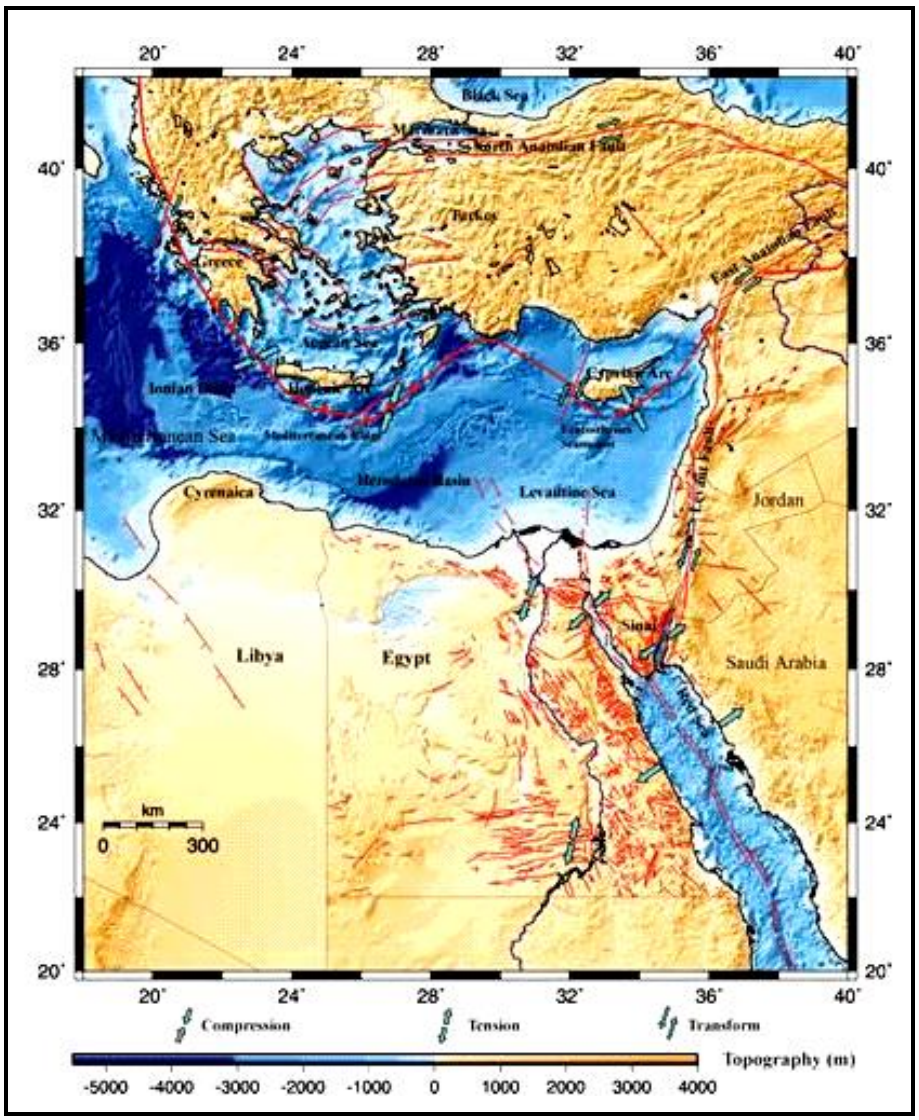

Fig. (4): Regional tectonic setting of the Eastern Mediterranean Region. A compiled map from Sofratome Group (1984), Abou Elenean (1997), Reilinger et al., (2000), Egyptian Geological Survey (1981) and Salamon et al., (1996).

There is a low activity to the north of the arc, hence the southern part of the Aegean sea is moving as a relatively rigid block when compared with the surrounding zones (McKenzie, 1978). The seismicity of the Eastern Hellenic arc is more diffusing and higher than the Western Hellenic arc, which may be due to a seismic gap or the activity of the arcs which depends on the thickness of sediments on the top of the subducted plate.

The spatial distribution of the earthquake hypocenters (60 <h <300 km) on the Hellenic arc (Korrat et al., 1996) indicates that, the subduction of the African plate under the Eurasian plate took place at an angle of about 30° and reaches a maximum depth of about 200 km.

The focal mechanisms of shallower earthquakes (Table.1) occurred in the convex side of Hellenic arc show a pure reverse faults and reverse faults with strike slip components (Fig. 4). The main trend of P-axis is in SW-NE direction (Figs. 5 and 6), which is almost perpendicular to the arc in its northwestern part but tends to become parallel to it in its southeastern part. The focal mechanisms for some events, which occur either in the convex side or in the concave side, show normal faults or normal faults with strike slip component. The trend of T-axis for these events takes the same direction of the dipping slab in western Hellenic arc and rotates to become in NW-SE direction in eastern Hellenic arc. Papadopoulos et al. (1986) explained the occurrence of these events in the convex side due to bending down of the subducted slab. In the western Hellenic arc most of the movement is approximately down dip movement with the dip angle increasing with the depth of events (Korrat et al., 1996), while in eastern Hellenic the strike slip movement increased. This phenomenon is probably due to the rotation of southwestern Turkey. The dominant focal mechanisms of the concave side of the arc are normal faulting which is related to the extensional stress field due to the back arc activity behind the arc, (Figs. 5 and 6). Figure (7) shows the stress tensor directions of the Hellenic arc.

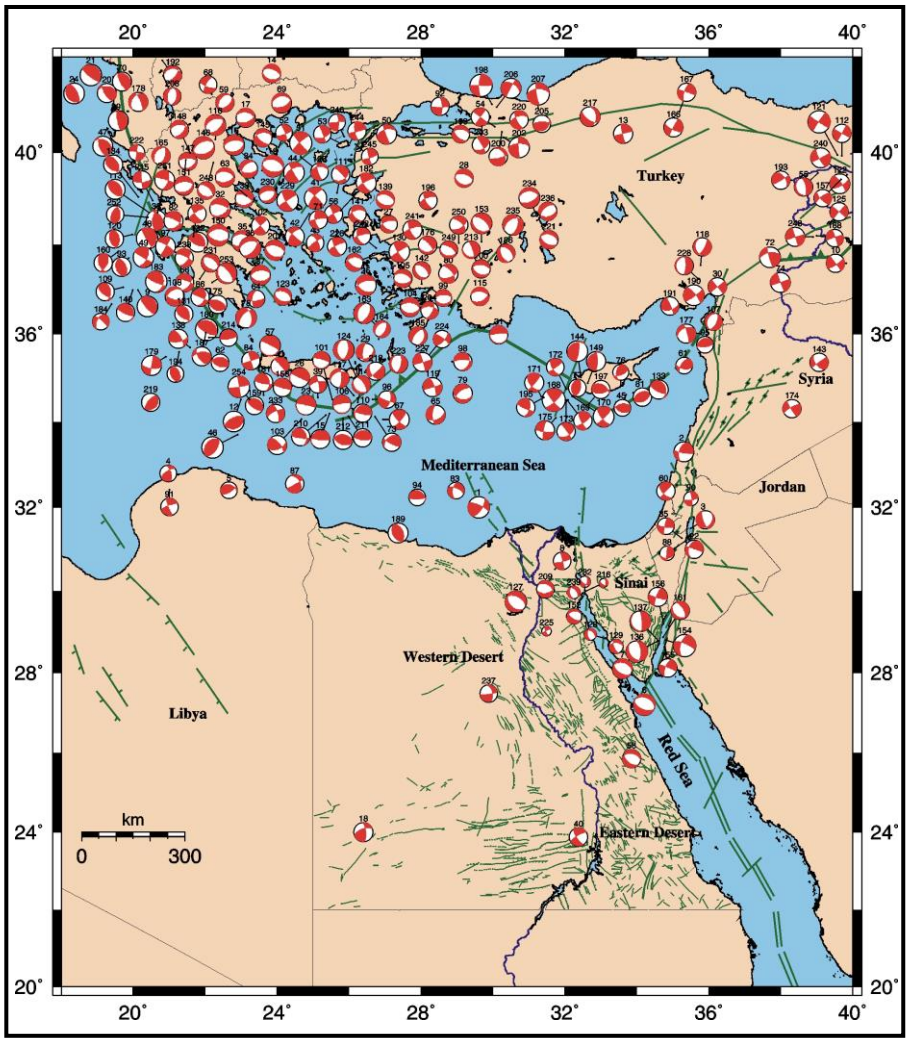

Fig. (5): Focal mechanisms for shallow earthquakes in the Eastern Mediterranean and the northern red Sea Regions (h<60 km). Red quadrant denotes compression.

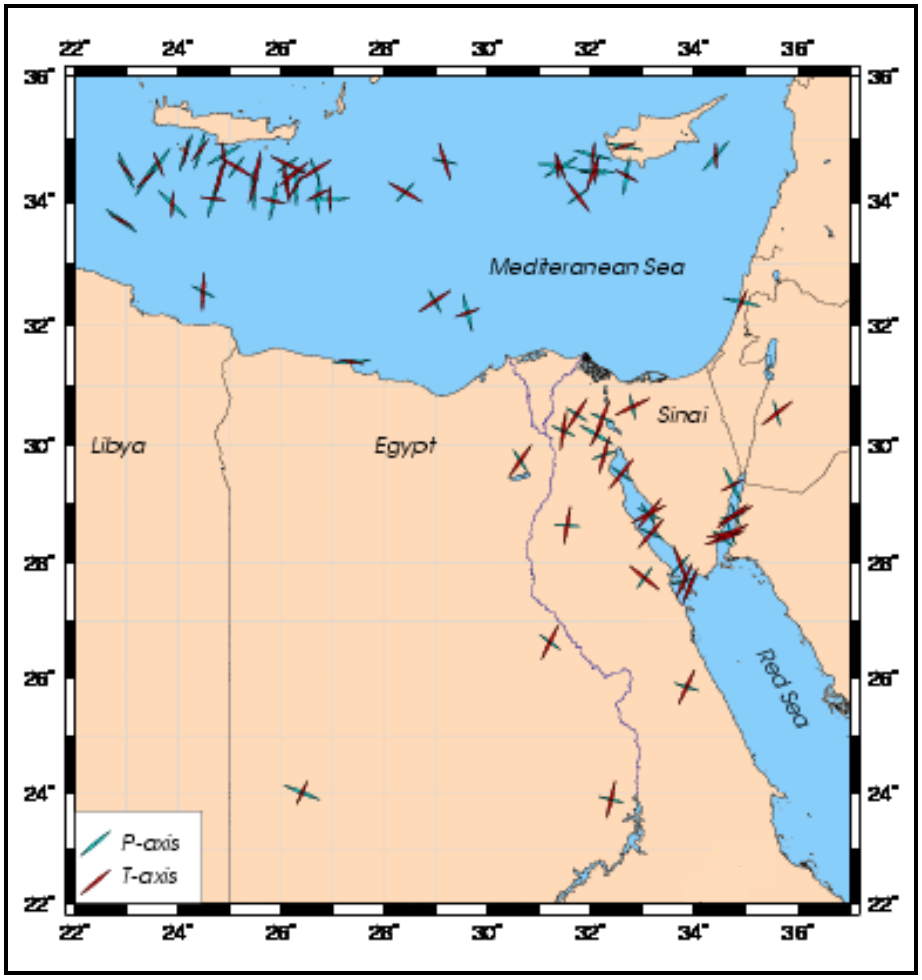

Fig. (6): Spatial Distribution of the Stress Axes Derived from the Focal Mechanisms of Moderate to large Earthquakes. Symbol Length is proportional to the dominant one.

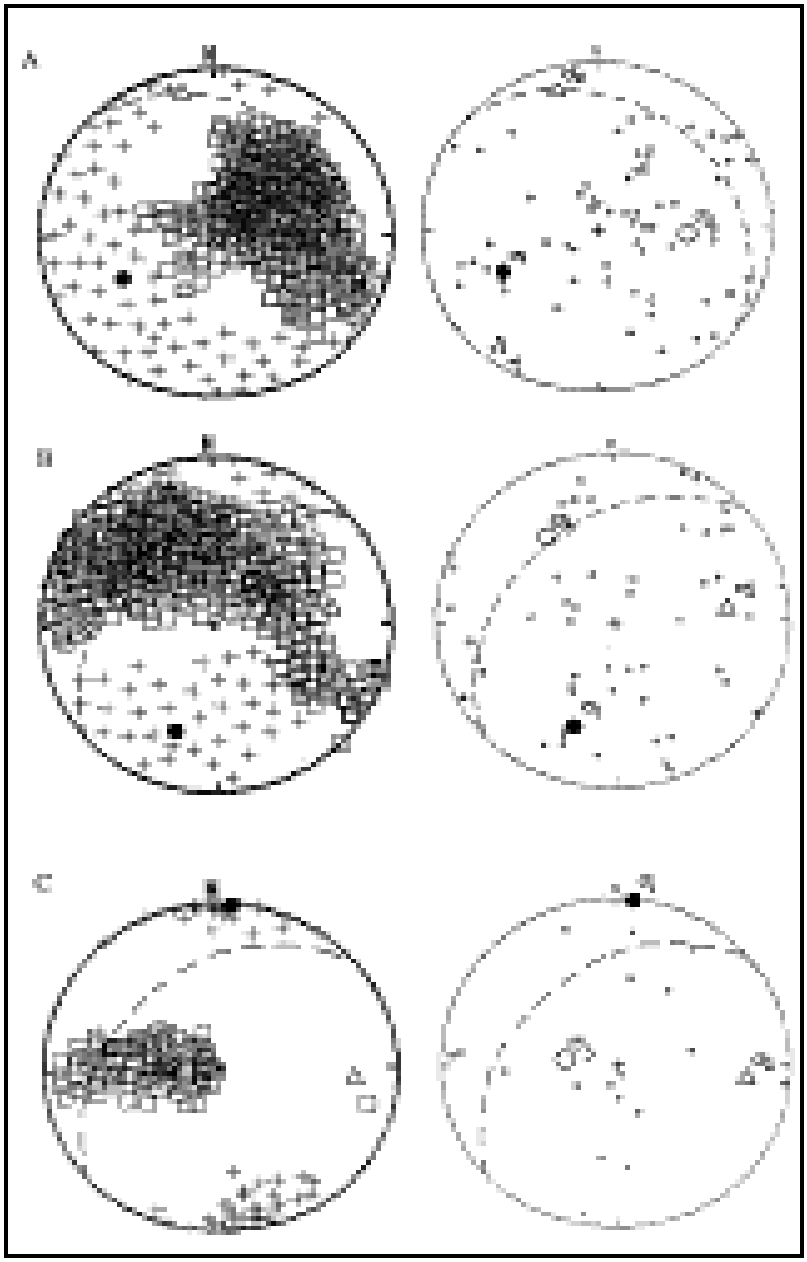

Fig. (7): Stress Tensor Directions of the Hellenic Wadatic-Benioff Zone projected onto a lower Hemisphere for western flank (A), eastern flank (B) and lower part of the eastern flank (C).

iii. Seismicity and Focal Mechanisms of the Cyprian Arc

Seismic activity along this arc occurs in a wide seismogenic belt, which suggests that the plate border is a zone of deformation instead of single line. The seismicity follows the arcuate pattern of the arc (Fig. 3). Most of the seismic activity took place in southern Cyprus, few of them occurred in the NW direction and very few in the NE of it. McKenzie (1970, 1972) concluded from a regional earthquake analysis that convergence took place in a north-south direction along most of the Cyprean arc and suggested that a left lateral motion could take place along its easternmost segment curving towards northeast. A continuous zone of seismicity can be traced from Cyprus into Zagros Mountain together with the subparallel seismic zone in Syria (Rotstein and Ben-Avraham, 1985). They also suggested that the lower level of recent and historical (Ambraseys, 1978) seismicity in the easternmost Mediterranean may represent a seismicity gap. This gap will eventually be filled and this gap can be explained by a plate configuration, which will require only a small motion across this segment of the plate boundary.

The seismic activity of southern Cyprus are relatively shallow and may not exceed 100 Km. The occurrence of earthquakes deeper than 100 Km prompted to suggest a zone of subduction in this region (McKenzie, 1972). Papazachos and Comninakis (1978) suggested that the pattern of seismicity west of Cyprus is continuous and that a Benioff zone dipping to the north exists across the entire Eastern Mediterranean.

Rotstein and Ben-Avraham (1985) drew three cross sections for the intermediate seismicity of the Levantine basin, two of which are in the Gulf of Antalya and are nearly perpendicular to each other and one across Cyprus. The depth of the observed seismic activity increases from Cyprus to the Gulf of Antalya and dip approximately northwards indicating a simple subduction process in agreement with Buyukasikoglu (1980). The maximum depth of the subducted lithosphere reaches about 80-100 Km in central Cyprus but it is deeper than 100 Km beneath central Anatolia. The subduction zone in central

Cyprus dips to the NNW with an angle about 25°-30° similar to the Hellenic arc. Rotstein and Ben-Avraham (1985) interpreted the deep seismicity in the Gulf of Antalya to an earlier subduction, which was active prior to the collision of the Anaximander block and continues to be active today.

The Cyprian arc is generally characterized by thrusts and shear mechanisms, with one of their nodal planes being sub-parallel to the strike of the arc (Salamon et al, 2003). Many of the events with shear mechanisms are located southwest of Cyprus. East of Cyprus towards the northern Mediterranean triple junction show both tension and compression with shear component. The Focal mechanisms of few events in Southern Cyprus show either reverse faults or reverse faults with small strike slip components (Abou Elenean, 1993). The direction of the P-axis is NW-SE, which is perpendicular to the arc in its eastern and central parts, but oblique to its western part. The focal mechanisms (Table 1) of some events (Figs. 5 and 6), located in the western part of the Cyprian arc, show strike slip faults with small reverse or normal components. The two nodal planes are trending NNW- SSE and NE-SW. The stress tensor analysis for the Cyprian Arc earthquakes indicates to NW-SE trending P-axis, (Fig. 8).

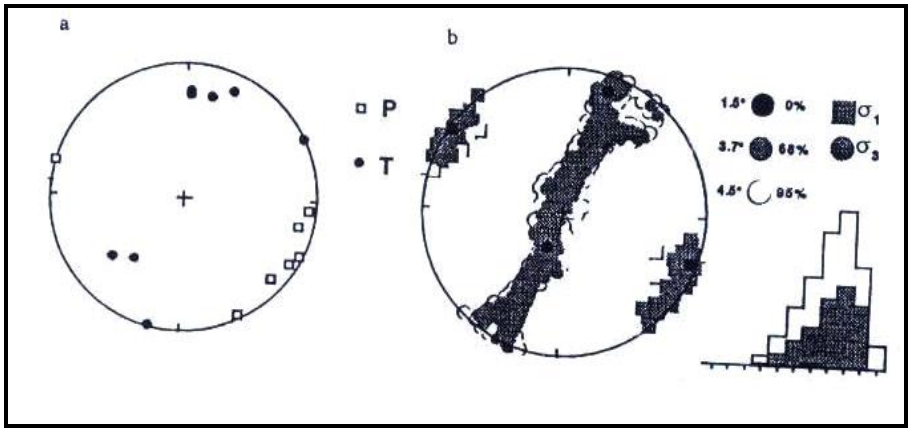

a- The distribution of P- and T- axis b- Best fit stress model.

Fig. (8): The best fit stress model for the Cyperian arc.

Table (1): Focal mechanism parameters of moderate to large shallow earthquakes occurred recently in the Eastern Mediterranean region.

No.	Date			Time			Location		Focal Mechanism			H	mb	Ref.
	Yr.	M.	Day	H.	Mn.	Sec	Lat.	Long.	St.	dip	rake	(km)		
1	1955	09	12	06	09	24	32.00	29.60	294	73	152	33	6.1	K96
2	1956	03	03	19	43	28	33.30	35.30	100	80	141	33	5.5	S03
3	1956	12	18	17	53	00	31.50	35.50	161	71	−114	33	5.2	S03
4	1963	02	21	17	14	31	32.69	20.97	237	67	147	33	4.6	K96
5	1967	01	02	08	19	37	32.40	22.66	059	69	066	33	4.6	K96
6	1969	03	31	07	15	54	27.61	33.91	112	53	−091	06	6.1	H87
7	1972	06	28	09	49	35	27.70	33.80	121	50	−082	06	5.5	H87
8	1974	04	29	20	04	39	30.52	31.72	347	84	−008	33	4.8	H90
9	1976	05	11	16	59	48	37.56	20.35	339	14	110	33	5.8	CMT
12	1977	09	11	23	19	23	35.05	23.03	074	28	100	33	5.8	CMT
15	1978	03	07	22	33	46	34.50	25.26	225	14	040	42	5.4	CMT
16	1978	05	23	23	34	11	40.76	23.27	074	36	-096	10	5.7	CMT
18	1978	06	20	20	03	22	40.78	23.24	354	68	032	03	6.1	CMT
22	1979	04	23	13	01	58	31.24	35.46	197	40	-004	33	5.1	CMT
23	1979	05	15	06	59	21	34.53	24.44	172	04	-020	33	5.6	CMT
26	1979	06	15	11	34	15	34.96	24.24	216	11	010	33	5.6	CMT
29	1979	07	23	11	41	54	35.48	26.32	061	35	-040	33	5.2	CMT
37	1981	03	07	11	34	43	38.19	23.32	091	40	-084	33	5.5	CMT
39	1981	09	13	23	25	27	34.85	25.06	256	65	-011	44	4.8	CMT
40	1981	11	14	09	05	29	23.69	32.60	146	72	-015	10	5.1	CMT
45	1982	05	20	03	28	10	34.62	33.70	261	48	069	33	4.6	S03
46	1982	08	17	22	22	21	33.73	22.97	219	34	093	10	6.0	CMT
57	1984	06	21	10	43	40	35.35	23.29	079	07	−128	27	5.7	CMT
58	1984	07	02	01	46	58	25.25	34.57	281	45	−110	10	5.1	CMT
60	1984	08	24	06	02	24	32.71	35.16	134	56	000	28	5.0	K96
61	1984	12	18	13	59	34	35.29	35.32	215	58	042	33	4.7	S03
62	1985	04	21	08	49	40	35.68	22.20	269	36	071	36	4.9	CMT
64	1985	05	23	16	02	22	36.60	22.22	186	55	−159	39	4.8	CMT
65	1985	07	22	21	32	27	34.39	28.30	067	48	-034	15	5.4	CMT
66	1985	09	07	10	20	50	37.48	21.24	040	44	−147	33	5.2	CMT
67	1985	09	27	16	39	48	34.51	26.59	135	76	013	59	5.5	CMT
73	1986	05	22	19	52	19	34.51	26.59	227	37	024	30	5.1	CMT
75	1986	06	08	04	55	01	36.07	21.51	109	34	086	29	5.1	CMT
76	1986	07	07	14	17	26	34.83	33.55	068	65	127	50	4.5	K96
77	1986	07	30	02	12	56	34.68	32.34	014	57	092	36	4.8	K96
79	1986	10	02	10	12	39	34.63	28.36	099	37	-053	10	5.3	CMT
81	1987	01	15	11	19	34	34.67	33.90	062	48	087	34	5.0	K96
83	1987	04	09	03	00	04	32.39	28.97	186	56	-030	10	4.6	CMT
84	1987	04	12	02	47	18	35.43	23.43	252	90	180	33	5.1	CMT
85	1987	04	27	20	41	47	31.27	35.25	191	80	010	09	4.7	S03
86	1987	06	10	14	50	11	37.23	21.45	024	44	180	37	5.0	CMT
87	1987	06	28	00	50	15	32.75	24.37	326	40	-007	10	5.2	CMT
88	1987	10	23	16	32	35	31.19	35.34	184	84	058	07	4.1	S03
90	1988	01	13	00	03	00	32.20	35.50	352	80	-014	10	4.1	S03
91	1988	01	28	15	48	07	32.33	21.20	251	75	-169	10	4.8	CMT

Table (1): Continue.

No.	Date			Time			Location		Focal Mechanism			H	mb	Ref.
	Yr.	M.	Day	H.	Mn.	Sec	Lat.	Long.	St.	dip	rake	(km)		
93	1988	05	18	05	17	43	38.42	20.47	163	38	095	32	5.3	CMT
94	1988	06	09	02	18	24	32.23	27.90	087	71	077	10	4.7	CMT
96	1988	09	05	20	03	25	34.51	26.65	015	55	-011	12	4.9	CMT
98	1988	11	20	21	01	05	35.29	28.67	024	32	-152	10	5.2	CMT
101	1989	03	17	05	42	51	34.64	25.59	077	10	-118	17	4.8	CMT
103	1989	03	28	13	29	11	34.06	24.68	067	53	029	33	5.4	CMT
106	1989	06	14	18	06	37	34.30	26.10	102	08	-068	10	5.1	CMT
108	1989	08	20	18	32	30	37.28	21.21	237	37	-130	16	5.4	CMT
109	1989	08	24	02	13	13	37.96	20.21	356	38	131	16	5.0	CMT
110	1989	08	27	01	21	17	34.92	26.26	223	19	033	60	5.0	CMT
114	1990	07	09	11	22	17	34.92	26.75	129	27	-106	33	5.1	CMT
117	1991	03	19	12	09	24	34.82	26.28	245	36	-033	18	5.4	CMT
119	1991	10	18	14	04	54	35.76	28.64	341	73	177	33	5.3	CMT
124	1992	04	30	11	44	38	35.07	26.71	172	38	-106	17	5.7	CMT
125	1992	05	07	19	15	02	38.68	40.13	310	90	-180	10	5.0	CMT
126	1992	07	23	20	12	42	39.82	24.39	267	41	-160	07	4.9	CMT
127	1992	10	12	13	09	56	29.89	31.22	136	42	-075	25	5.9	A97
128	1992	10	27	09	04	46	28.84	33.11	171	51	-063	10	3.4	A97
129	1992	10	27	11	02	44	28.85	33.12	158	66	-046	19	3.9	CMT
131	1993	03	05	06	55	08	37.15	21.44	342	42	120	37	5.2	CMT
133	1993	03	22	11	03	40	34.74	34.41	343	27	133	10	5.3	CMT
136	1993	08	03	12	43	04	28.63	34.64	139	36	-122	10	6.0	CMT
137	1993	08	03	16	33	20	28.76	34.70	142	13	-123	10	5.7	CMT
138	1994	01	11	07	22	51	35.95	21.91	077	61	030	33	5.3	CMT
140	1994	04	16	23	09	33	37.44	20.58	340	18	134	23	5.2	CMT
144	1995	02	23	21	03	02	35.04	32.27	239	21	140	15	5.8	CMT
149	1995	05	29	04	58	32	35.06	32.26	224	20	132	10	5.3	CMT
152	1995	09	08	12	13	22	29.48	32.25	123	65	-065	13	4.2	A97
154	1995	11	22	04	15	11	28.82	34.86	196	59	-015	10	6.2	CMT
155	1995	11	22	22	16	53	28.45	34.84	202	67	-003	10	5.0	CMT
156	1995	11	23	18	07	17	29.25	34.64	199	77	007	10	5.3	CMT
158	1995	12	07	18	00	50	34.79	24.15	319	06	123	00	5.2	CMT
160	1996	02	01	17	57	55	37.76	19.86	156	48	049	10	5.2	CMT
161	1996	02	21	04	59	51	28.80	34.78	132	30	-104	10	5.1	CMT
168	1996	10	09	13	10	52	34.56	32.13	048	77	170	33	6.4	CMT
169	1996	10	09	14	00	10	34.49	32.06	152	74	018	33	5.2	A97
170	1996	10	09	14	19	37	34.59	32.20	046	79	159	33	5.7	A97
171	1996	10	10	01	10	22	34.56	32.21	139	53	012	33	5.4	CMT
172	1996	10	10	04	54	46	34.85	32.29	147	62	004	33	4.9	CMT
173	1996	11	27	00	44	23	34.50	32.06	062	48	-168	33	5.0	CMT
175	1997	01	13	10	19	26	34.31	32.33	097	76	-011	33	5.3	CMT
179	1997	07	27	10	07	52	35.58	21.06	098	65	180	33	5.5	CMT
180	1997	10	13	13	39	37	36.38	22.07	298	20	089	24	6.2	CMT
181	1997	11	05	12	22	55	34.77	23.98	350	34	154	33	5.1	CMT
184	1997	12	02	19	22	44	36.02	19.66	206	49	-020	33	4.7	CMT
185	1998	03	09	11	21	20	36.02	28.39	010	33	-116	72	5.1	CMT

Table (1): Continue.

No.	Date			Time			Location		Focal Mechanism			H	m	Ref.
	Yr.	M.	Day	H.	Mn.	Sec	Lat.	Long.	St.	dip	rake	(km)	b	
187	1998	04	29	03	30	39	36.14	21.94	260	53	036	33	5.3	CMT
189	1998	05	28	18	33	28	31.40	27.67	154	44	089	10	5.5	CMT
194	1999	04	17	08	17	58	36.04	21.68	160	43	095	40	4.7	CMT
195	1999	05	25	17	15	21	34.48	32.13	014	53	165	10	5.2	CMT
197	1999	08	11	04	27	55	34.79	32.94	303	42	124	33	5.1	CMT
209	1999	12	28	12	05	10	30.24	31.46	296	43	-064	15	4.8	A04
210	2000	02	22	11	55	25	34.60	25.60	347	34	157	33	5.1	CMT
211	2000	03	10	22	01	46	34.36	26.03	256	22	072	10	5.1	CMT
212	2000	04	05	04	36	58	34.22	25.69	276	43	080	38	5.3	CMT
213	2000	04	21	12	23	10	37.84	29.33	110	23	−139	33	4.9	CMT
214	2000	05	24	10	01	44	35.92	22.10	263	12	093	33	4.9	CMT
216	2000	06	01	16	44	83	29.99	32.58	003	54	-041	06	2.5	A04
218	2000	06	13	01	43	14	35.15	27.12	147	45	−166	10	5.2	CMT
223	2001	05	01	06	00	56	35.70	27.50	176	25	−105	33	5.1	CMT
224	2001	05	29	04	43	57	35.41	27.78	042	66	013	20	4.9	CMT
225	2001	06	09	00	25	25	29.02	31.49	155	75	-013	5.	2.6	A04
227	2001	06	23	06	52	43	35.55	28.16	344	85	177	50	5.4	CMT
231	2001	09	16	02	00	47	37.24	21.87	130	40	-086	10	5.0	CMT
232	2001	10	16	07	38	09	30.02	32.55	013	52	-036	15	3.1	A04
233	2001	11	26	05	03	21	34.82	24.28	343	69	−158	33	5.1	CMT
235	2002	02	03	09	26	43	38.63	30.90	236	45	-058	10	5.7	CMT
237	2002	09	18	14	56	59	27.49	29.88	347	53	-010	10	4.8	A04
239	2002	12	05	02	21	48	29.96	32.24	171	41	-067	24	3.6	A04
245	2003	07	06	20	10	16	40.42	26.13	073	77	173	17	4.7	CMT
253	2004	03	17	05	20	56	34.50	23.50	081	87	-180	33	6.0	CMT

A97: Abou Elenean, 1997; S03, Salamon et al., 2003, K96 : Korrat et al., 1996
H90: Hassib, 1990, H87: Huang and Solomon, 1987, CMT: Harvard solutions.

iv. Seismicity and Focal Mechanisms of the Northern Red Sea-Gulf of Suez

The epicentral distribution map (Fig. 3) show that the seismic activity in the northern Red Sea is clustered at the entrance of the Gulf of Suez and the activity continues southward in the medial of the Red Sea. The cluster of the activity at this point may be due to the intersection of NW (Gulf of Suez -Red Sea) faults with the Aqaba trend. Few events are located in the central Red Sea almost at the transform faults crossing the rift axis.

Pedone et al. (1992) suggested that the seismic activity of the northern Red Sea can be related to the dislocations of transform (mainly NE-SW) and normal faults associated with the down dropping

of blocks into the trough and to magmatic intrusions in the faulted Precambrian crust. The seismic activity extends to the north along the Suez rift and includes the northern part of the Eastern Desert. This trend is the major active trend inside the land of Egypt and extends towards Cairo and Alexandria toward northwest in the Mediterranean Sea.

The activity of this trend is attributed to the Red Sea rifting as well as to several active faults, which have trends NNW Parallel to the Red Sea-Gulf of Suez direction and its continuation toward East Mediterranean. Sofratome Group (1984) Supposed the possibility that Cairo- Alexandria fault zone (Fig. 4) absorbs the main effects of internal deformation in the northeast corner of Africa. This would rule out the occurrence of large earthquakes (M>6) to the west of Alexandria. Also they suggested that this fault zone separate two different tectonic regimes especially in the Pliocene-Quaternary of the Eastern and Western Nile Delta. Field observation, landsat images and seismic profiles confirm this suggestion indicating active tectonics in the Eastern Desert between Suez and Cairo compared with the Western Desert of Egypt.

The focal mechanisms of few events along the northern Red Sea (Abu Eleneen, 1997) reflect normal faulting mechanism predominantly have nodal planes parallel to the rifting direction. Some of the focal mechanisms show a strike slip movement, which may be related to the events located at the transform faults that crossed the main rift direction, (Figs. 5 and 6). The stress tensor inversion for few earthquakes along the northern part of the Red Sea (Abou Elenean, 1997) show a stress axes σ_1, σ_2 and σ_3 directed azimuth/plunge 202/59, 318/15 and 56/27 which reflect a dominant tension stress (Fig. 9).

The focal mechanisms of few events have small to moderate size along the Gulf of Suez-Northern part of the Eastern Desert show normal faults with small component of strike slip movements. The strike slip component increased on land than a long the Gulf area. The

fault planes are generally trending ENE-WSW to E-W and NNW-SSE to NW-SE (Abou Elenean, 1997). The Stress axes σ_1, σ_2 and σ_3 are trending azimuth/plunge 105/39, 341/34 and 226/32 respectively (Fig 10). This stress model reflects a dominant tension stress with considerable amount of strike slip components.

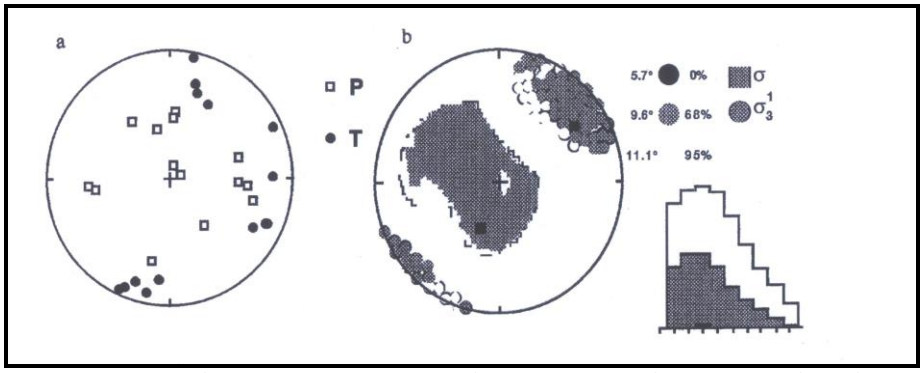

(a) The Distribution of the P- and T- axes; (b) best fit stress model, confidence ranges of the fit and histogram reflect the tested numbers of the stress models for different confidence limits.

Fig. (9): The best fit stress model for the northern Red Sea part.

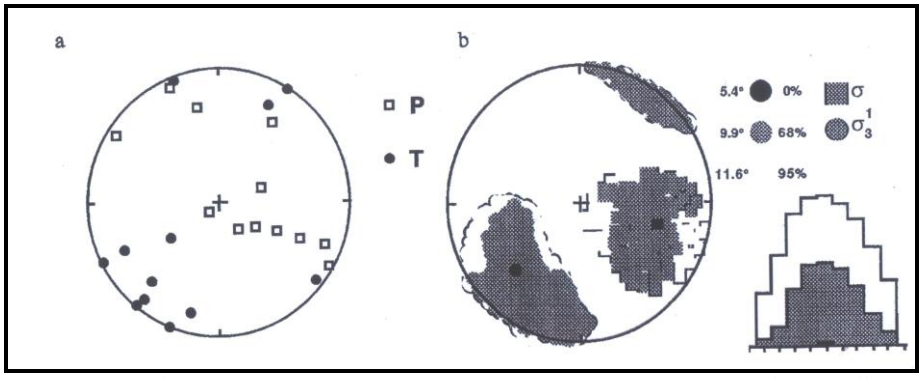

(a) Distribution of the P- and T- axes. (b) Best stress model with the other solutions for the different confidence limits and histogram reflect the numbers of the stress model inside different confidence ranges.

Fig. (10): Stress tensor inversion for the Gulf of Suez-northern eastern desert.

Bosworth and Taviani (1996) concluded by analyzing borehole breakouts and mesoscopic fault arrays a dominant NNE-SSW extension stress. Northwest the Gulf of Suez, and outside the rift province the destructive 10/92 Cairo earthquake is most important. Its extensional mechanism combined with slight shear component, fits well with both the Suez rift system and the E-W transverse normal faults east of Cairo.

v. Seismicity and Focal Mechanisms of the Aqaba-Levant Transform fault

The seismic activity of this fault zone is relatively high (Fig. 3) and may be attributed to some local reasons as the upwelling magmas or the intersection of two or more tectonic elements (Fig. 4). The activity is trending NNE along the main fault of the Gulf and changed toward the north until Taurus. The activity is diffused in some places due to the intersection of transverse faults with the NNE main trend.

From previous focal mechanism solutions along this trend, the main trend of T-axis is in N51°E and for P-axis is N65°W (Abou Elenean, 1993). The focal mechanism solutions (Figs. 5 and 6) along this trend reflect strike slip faults predominantly with normal components. Few events on the eastern side of the Aqaba Gulf (northwestern part of Saudia Arabia) and to the north (southern Lebanon, northern Syria) show strike slip with reverse component. The solutions give nodal planes trending N-S to NNE-SSW (main fault trend) and NNW-SSE to ESE-WNW (transverse faults). These mechanisms can be interpreted as they are related to pull apart faulted basins directed mainly N-S and encountered by transverse faults along E-W or ESE-WNW.

The stress tensor inversion along the Aqaba Gulf gave stress axes σ_1, σ_2 and σ_3 trending azimuth/plunge 333/27, 114/56 and 233/18 (Fig. 11) which indicate a dominant strike slip movement with normal component (Abou Elenean, 1997). Various mechanisms appears at the juncture zone of Sinai, Arabia and Anatolia where the Dead Sea transform, the East Anatolian Fault and the Cyprina arc meet

(Salamon et al., 2003). The overall deformation of the Arabian-Anatolian boundary seems to separate into two components; a left lateral shear which is absorbed on ENE-striking faults and an NW thrusting on either steep or shallow dipping planes. Furthermore, an extension regime is found amid the shear and thrust, possibly related to the Iskendrun Bay. Salamon et al (2003) indicated that all earthquakes along the Dead Sea transform exhibit mainly sinistral transtension and transpression, reflecting its leaky manner and local change in the transform geometry. The presence of other unexpected mechanisms near the transform reflects the heterogeneous deformation it induces around.

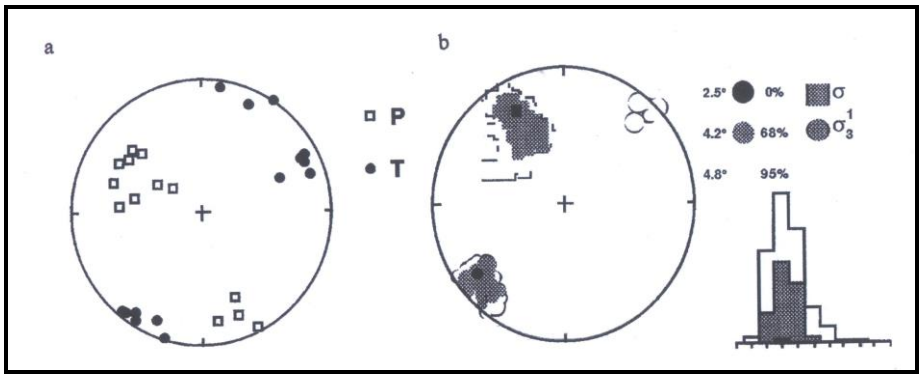

(a) Distribution of the P-an T- axes. b: best stress model with the other solution for different confidence limits and histogram reflects the numbers of the stress models within different confidence ranges.

Fig. (11): Stress trensor inversion for the Gulf of Aqaba zone.

vi. Seismicity and Focal Mechanisms of Southern Red Sea and Yemen Territories:

Previous works on the focal mechanism analysis in Yemen are very limited in number due to the small number of large events to be solved. Besides there did no seismic stations exist before 1994. There are many ways to determine the earthquake focal mechanism, one of them is done by using the polarity data of the recorded P and S waves and another one is done by the inversion of their recorded waveform. Figure (12) shows the seismic activity in Yemen.

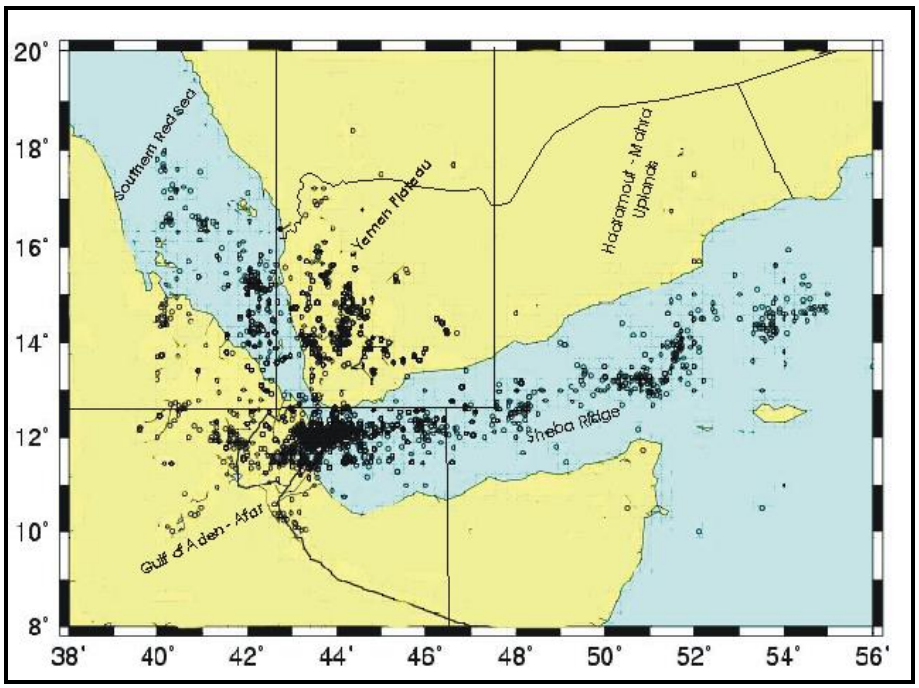

Fig. (12): Epicentral distribution of Yemen and surrounding areas for the period From 1975 to 2003.

The interpretation of the seismic activities were evaluated through the collected focal mechanisms that were done by previous works and that have been published by the world data centers (Harvard CMT) beside, the analysis and interpretation of our team. The studied area is divided into regional and local seismic zones (Fig. 13).

C) Regional mechanism

The current tectonic setting of Yemen is best understood by considering the overall geological history and evolution of the Arabian plate, Somalian plate and the southern Red Sea rift. The most active tectonic features are along plate boundaries, where the deformations are large. The plate motion also controls the deformations within individual plates. Hence the present day tectonic deformations within Yemen are related to the regional tectonic forces and to the local tectonics of Yemen.

The stress field distribution represents a good key for understanding the tectonic situation and the direction of relative plate movements. The most common way for studying the seismotectonics of any specified region is done by plotting a stress field map on the basis of focal mechanisms, microtectonic analysis or in-situ stress measurements.

In this study about seventy eight (78) solutions by Harvard CMT have used to study the regional tectonic stresses. The parameters of these earthquakes are shown in tables (2) and (3). The focal mechanisms are projected using the lower hemisphere projection (Fig. 13).

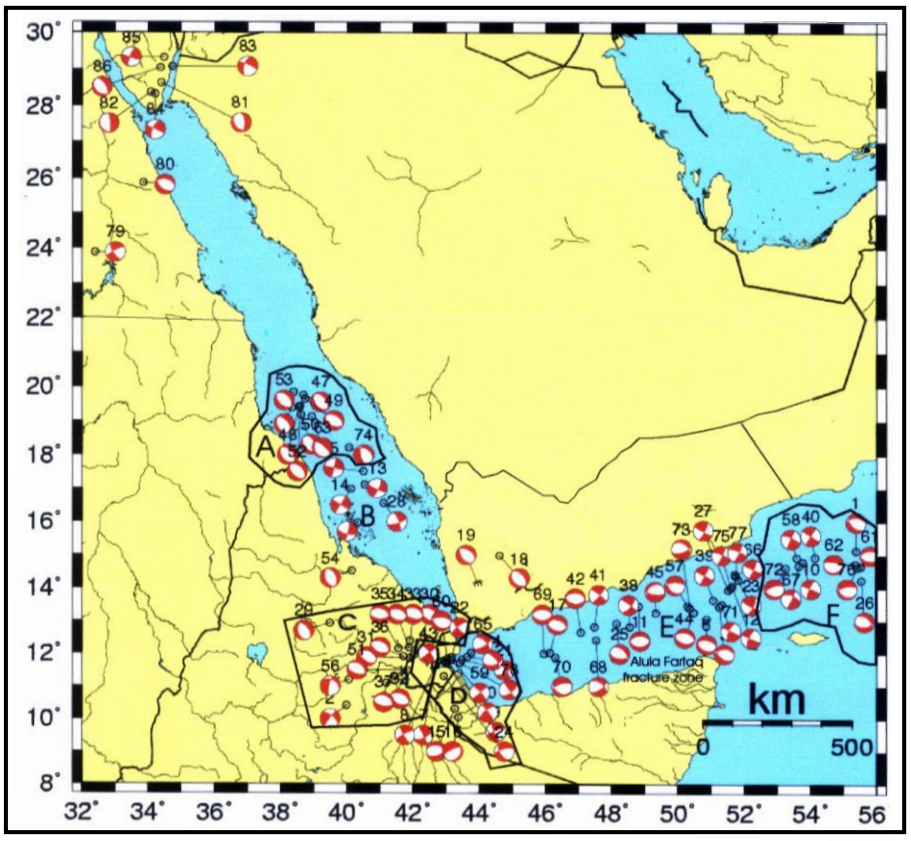

Fig. (13) : Focal Mechanism solutions and different seismic zones according to the (P-axis) and the Tension (T-axis) for the southern Red Sea and Yemeni Territories, (After A. Alaydros, 2003).

Table (2): The Chosen Earthquakes of Magnitude Larger Than 5 According to Richter Scale and used for the Focal Mechanism Solutions.

No.	Date	Lat.	Long.	Magnitude	Depth
1	1977/02/28	15.16	55.37	5.3	10.0
2	1977/07/08	10.42	39.98	5.3	15.0
3	1977/12/17	13.45	51.25	5.4	15.0
4	1977/12/28	15.97	40.32	6.6	10.1
5	1978/01/17	17.51	40.49	5.4	15.0
6	1978/02/11	13.08	50.86	5.7	15.0
7	1978/11/07	11.64	42.67	5.9	15.0
8	1978/11/08	11.66	42.67	5.8	15.0
9	1978/12/21	11.79	42.91	5.7	15.0
10	1979/07/08	14.81	53.77	5.9	15.0
11	1979/09/24	13.46	48.81	5.2	15.0
12	1979/12/22	14.07	51.64	5.8	15.0
13	1980/01/14	17.12	40.53	6.0	15.0
14	1980/01/14	16.99	40.12	5.7	15.0
15	1980/05/03	10.31	43.26	5.6	15.0
16	1980/05/30	10.05	43.37	5.3	15.0
17	1982/12/08	12.03	46.13	5.6	14.2
18	1982/12/13	14.99	44.60	6.2	10.1
19	1982/12/29	14.10	43.97	5.5	15.0
20	1983/09/28	11.71	43.01	5.3	15.0
21	1983/09/30	11.83	43.47	5.7	37.4
22	1983/10/19	11.91	43.17	5.4	10.0
23	1984/01/28	14.27	51.82	5.7	10.0
24	1985/06/04	11.31	42.93	5.1	10.0
25	1986/05/23	12.94	48.14	5.7	15.0
26	1987/06/16	14.25	55.53	5.0	15.0
27	1988/07/16	13.96	51.52	5.6	15.0
28	1988/12/10	16.56	41.10	5.6	15.0
29	1989/04/13	12.94	39.48	5.4	15.0
30	1989/08/20	11.99	42.04	6.5	15.9
31	1989/08/20	11.86	41.90	6.1	15.0
32	1989/08/20	11.32	41.42	5.7	15.0
33	1989/08/20	12.40	41.91	6.1	15.0
34	1989/08/21	12.19	41.88	6.4	15.0
35	1989/08/21	12.17	41.56	6.1	15.0
36	1989/08/21	11.92	41.71	5.8	15.0
37	1989/08/21	11.10	41.18	5.3	15.0
38	1989/11/24	12.83	48.55	5.5	15.0

Table (2): Continue.

No.	Date	Lat.	Long.	Magnitude	Depth
39	1990/09/14	13.66	51.06	5.5	15.0
40	1990/11/03	14.95	54.13	5.2	15.0
41	1991/05/11	12.84	47.48	5.4	15.0
42	1991/05/12	12.67	47.07	5.5	15.0
43	1992/03/05	11.75	42.98	6.2	15.5
44	1992/05/21	13.28	50.48	5.2	15.0
45	1993/01/08	13.26	49.33	5.5	15.0
46	1993/03/12	19.39	38.34	5.3	15.0
47	1993/03/12	19.76	38.68	5.0	15.0
48	1993/03/13	19.42	38.55	5.7	15.0
49	1993/03/14	19.65	38.74	4.9	15.0
50	1993/03/16	19.18	38.61	5.3	15.0
51	1993/03/16	11.49	41.82	5.6	15.0
52	1993/03/22	19.43	38.59	5.0	15.0
53	1993/03/23	19.85	38.39	5.2	16.3
54	1993/05/06	14.52	40.14	5.2	15.0
55	1993/08/01	15.37	31.35	5.5	15.0
56	1993/09/21	11.19	40.05	5.7	15.0
57	1993/10/12	13.48	50.29	5.2	15.0
58	1993/11/09	14.94	53.58	5.6	15.0
59	1994/04/11	11.82	43.15	5.9	15.0
60	1994/04/24	11.85	43.03	5.6	15.0
61	1995/12/07	14.68	55.52	5.3	15.0
62	1996/03/14	14.75	55.35	5.2	15.0
63	1996/11/02	19.13	38.94	5.3	15.0
64	1997/03/08	11.90	43.64	5.3	15.0
65	1997/03/09	12.04	43.75	5.5	15.0
66	1997/06/07	14.43	51.72	5.4	15.0
67	1998/10/01	14.69	53.65	5.6	15.0
68	1998/11/23	12.43	47.54	5.4	15.0
69	2000/02/10	12.01	45.95	5.1	15.0
70	2000/02/14	11.89	46.30	5.4	15.0
71	2000/06/24	13.52	51.32	5.3	15.0
72	2001/03/25	14.63	53.25	5.1	15.0
73	2001/04/23	13.41	50.35	5.3	15.0
74	2001/05/25	18.21	40.07	5.2	15.0
75	2001/06/15	14.03	51.59	5.9	15.0
76	2001/07/14	14.64	55.41	5.2	15.0
77	2001/08/26	14.38	51.74	5.6	15.0
78	2001/11/02	11.72	43.41	5.1	15.0

Table (3): The Extracted Parameters from the Focal Mechanism Solutions for the Chosen Earthquakes.

	Plane I			Plane II			P-axis		T-axis	
	Strike	**Dip**	**Rake**	**Strike**	**Dip**	**Rake**	**Azimuth**	**Plunge**	**Azimuth**	**Plunge**
1	274	048	-118	132	049	-063	112	70	203	01
2	310	066	-171	216	082	-024	171	23	265	11
3	270	045	-117	126	051	-066	100	71	199	03
4	106	066	-171	013	081	-024	327	23	061	11
5	282	090	180	012	090	000	147	00	057	00
6	116	039	-079	282	052	-990	151	81	018	06
7	064	065	-178	334	089	-025	286	19	221	19
8	150	080	-009	242	081	-170	106	13	016	01
9	155	076	-012	247	078	-166	112	18	021	02
10	203	080	178	293	088	010	068	06	159	08
11	268	045	-090	088	045	-090	088	90	178	00
12	204	073	-176	113	086	-017	067	15	160	09
13	024	076	-009	116	081	-166	341	16	250	04
14	301	090	180	031	090	000	166	00	076	00
15	280	040	-068	072	054	-107	090	74	175	07
16	022	023	-130	244	073	-075	176	60	322	26
17	105	039	-093	288	051	-088	215	84	017	06
18	134	037	-095	320	053	-086	248	81	048	08
19	303	043	-107	145	049	-075	120	78	225	03
20	232	067	174	324	084	023	096	12	191	20
21	058	067	-168	324	079	-023	279	24	012	08
22	232	074	-165	137	076	-017	095	22	185	01
23	025	069	170	118	081	021	249	08	342	22
24	149	054	-027	256	069	-140	118	42	019	09
25	314	044	-062	098	052	-114	307	70	204	04
26	310	049	-056	084	051	-123	289	65	197	01
27	028	076	175	119	085	014	253	06	343	13
28	339	074	-017	074	074	-163	296	23	026	00
29	168	039	-070	323	054	-106	184	75	064	08
30	301	045	-090	121	045	-090	121	90	211	00
31	288	038	-109	130	055	-076	086	76	211	08
32	294	045	-090	114	045	-090	113	90	204	00
33	285	034	-092	108	056	-089	022	79	196	11
34	281	045	-101	116	046	-079	105	82	199	01
35	290	041	-077	092	051	-101	309	80	191	05
36	296	045	-090	116	045	-090	116	90	206	00
37	296	032	-078	102	059	-097	351	75	197	13
38	041	067	-168	307	079	-024	262	24	355	08

Table (3): Continue.

	Plane I			Plane II			P-axis		T-axis	
	Strike	**Dip**	**Rake**	**Strike**	**Dip**	**Rake**	**Azimuth**	**Plunge**	**Azimuth**	**Plunge**
39	207	090	-180	297	090	000	108	00	197	00
40	212	090	-180	302	090	000	103	00	167	00
41	308	082	-008	040	082	-172	264	11	174	00
42	275	045	-090	095	045	-090	095	90	185	00
43	324	074	003	233	087	164	280	09	187	13
44	284	045	-090	104	045	-090	104	90	194	00
45	231	030	-134	099	069	-068	041	60	173	21
46	148	031	-083	320	059	-094	218	75	014	53
47	321	045	-090	141	045	-090	141	90	231	00
48	144	040	-084	316	050	-095	193	84	050	05
49	301	045	-090	121	045	-090	121	90	211	00
50	127	038	-114	335	056	-073	293	73	054	09
51	308	037	-076	110	055	-100	344	78	208	09
52	315	045	-090	135	045	-090	135	90	225	00
53	313	045	-090	133	045	-090	133	90	223	00
54	337	045	-090	157	045	-090	157	90	247	00
55	172	063	-014	269	077	-152	133	28	038	10
56	299	038	-159	192	077	-054	139	45	255	24
57	137	037	-048	269	063	-117	136	62	018	14
58	294	075	003	203	087	165	250	08	158	13
59	318	078	-002	049	088	-168	274	10	183	07
60	120	034	-067	273	059	-105	148	72	014	13
61	272	045	-090	092	045	-090	092	90	182	00
62	072	020	-118	282	072	-080	206	61	004	27
63	153	020	-068	310	072	-098	208	63	046	26
64	077	047	-143	320	064	-050	279	53	022	10
65	315	058	-024	058	070	-146	280	38	184	08
66	024	081	177	114	087	009	249	04	340	08
67	290	058	-009	025	082	-148	252	28	153	16
68	305	053	-033	056	064	-138	276	47	178	07
69	270	045	-090	090	045	-090	090	90	180	00
70	120	031	-052	257	066	-111	135	63	003	19
71	205	070	177	296	087	020	069	12	162	16
72	109	029	-056	251	066	-107	132	65	354	20
73	304	040	-045	072	063	-120	296	60	183	13
74	303	036	-128	167	063	-066	118	64	240	14
75	293	077	-007	025	083	-167	249	14	158	04
76	121	027	-053	261	069	-107	144	62	004	22
77	292	078	-013	025	078	-167	248	18	338	00
78	053	063	179	143	089	027	275	18	012	19

i. Southern Red Sea

The focal mechanism solutions of the events located in the southern Red Sea (group A) suggest pure normal faulting mechanism (Fig. 13), with a NNE-SSW trending tension axis (Fig. 14). These events took place along the rift valley region which is characterized by continuous sea floor spreading.

To the south of group A events, there is another group events (Fig. 13, group B) reflecting strike slip mechanisms. Events no. 13, 14 and 22 took place along one of the NNE-SSW transform faults. The plane trending NNE-SSW indicating left lateral motion along this transform fault. Event 28 took place along NNW-SSE trending fault to the west of the rift valley. The mechanism of this event reflects strike slip mechanism with a left lateral motion along a NNW-SSS trending plane. Some events took place to the east of the rift valley along a NNW-SSE trending fault. The focal mechanism of this event shows strike slip mechanism along the same trend with a right lateral motion.

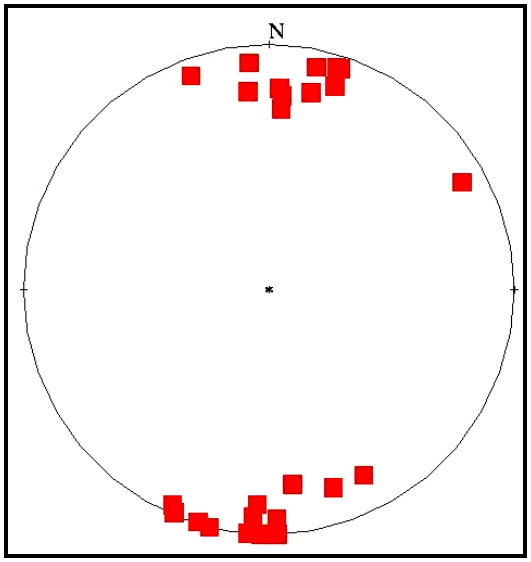

Fig. (14): Shows the NNE-SSW Trending Tension Axis in the Southern Red Sea.

ii. East African Rift (EAR)

The focal mechanism of events along the EAR spreading (group C) system indicates typical normal faulting mechanism for most parts (Fig. 13) with an average tension axis oriented NE-SW (Fig. 15) reflecting a continental divergent plate boundary.

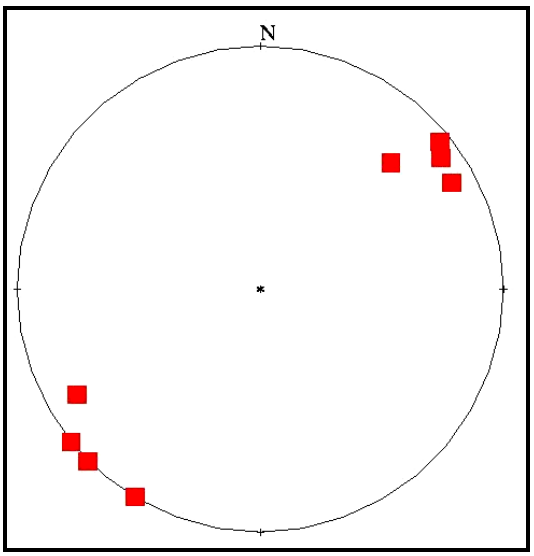

Fig. (15): Shows the Average Tension Axis oriented NE-SW in the East African Rift Reflecting a Continental Divergent Plate Boundary.

iii. Gulf of Aden

Generally the focal mechanism solutions in the Gulf of Aden (Fig.13) region shows two types of faulting normal and strike slip. Normal faulting mechanisms are associated with the spreading while the strike slip ones are related to the existing transform faults. The average direction of the tension axis in the Gulf of Aden is NNE-SSW (Fig. 16).

For the events that took place at the extreme west of the Gulf of Aden (Tadjura Gulf), (Fig. 13, group D). The majority of the epicenters are associated with the transform faults suggesting strike slip mechanism with a dip slip component.

The presence of such a mechanism reflects a westward extension of the transform fault system and extensional mechanism existing in the Gulf of Aden.

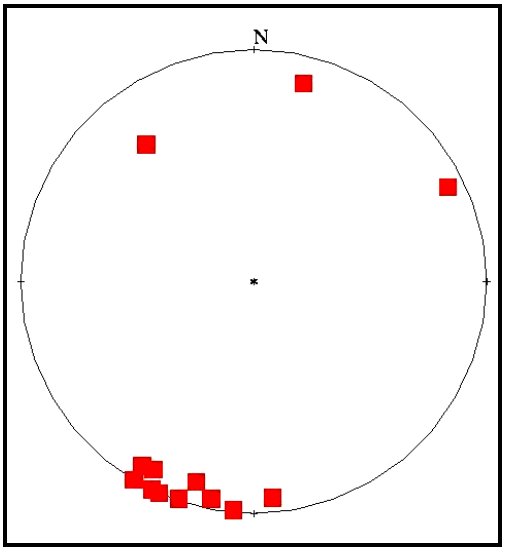

Fig. (16): Shows the Average Direction of the Tension Axis in the Gulf of Aden as NNE-SSW.

iv. Sheba -Ridge

The seismic activity along this zone is aligned conformably along the main rift axis nearly NWW-SEE. The activity also shows that the rift axis have been transformed by some NE-SW right central strike slip faults. The focal mechanisms (Fig. 13) indicate two types of fault mechanisms, the first shows a normal faulting mechanism while the second is strike slip faults. The normal faulting is trending nearly E-W along Sheba Ridge, (events no. 1, 61, 76, 26, 62), (group F). The events no. 40, 58, 10, and 67 indicate NE-SW transform faults that bisect the Sheba Ridge. The focal mechanism of events no. 12, 23, 66, 77, 75, 27 and 71 identify strike slip faults That is obvious from the group located to the right from group E. These events are in coincidence with the Alula-Fartak transform fault which has been reflected by previous magnetic and gravity studies.

v. Gulf of Aden-Afar rift mechanism

The fault plane solution of events no. 6, 44 and 57 reflect normal faults trending NW-SE in agreement with the Aswad ridge direction, figure (13). The extension that caused this ridge has extended toward north inland inside Yemen as reflected by the existence of Ataq-Balhaf Trough and Hajr Trough, the mechanisms numbers 67, 69 and 70 indicate normal faulting parallel to the main rift towards Afar. Along the Afar area the solution of about seven events show a normal faulting mechanism that tends to change its direction from E-W to NW-SE close to the Red Sea.

vi. Southern Red Sea

The focal mechanisms of the events lying along the southern part of the Red Sea show two types of faults, figure (13). The first one from the south indicates normal faulting with large strike-slip components. These solutions have two planes trending NE-SE and NE-SW as clearly shown for events no. 4, 3, 13 and 14. The second solution along the southern Red Sea reflects pure normal faulting trending parallel to the Red Sea direction (NW-SE), (see solution of Events No. 48, 49, 50, 52, 63 and 74).

D) Stress field

The stress fields based on the previous focal mechanism of the different seismic zones according to our study have been selected and the average direction of pressure axis (P-axis) and tension axis (T-axis) are calculated for each zone. The source parameters of these focal mechanisms are listed in table (3).

The distribution of the P and T axis for the Gulf of Aden- Afar rift shows a dominant T-axis directed N 25º E. Also, the T-axis is more horizontal and dominant along the Southern Red Sea part and trending N 45º E.

Volcanic activity and high geothermal activity characterize the Yemen region. Also the surface faults and dykes suggest extension stresses act in the region. Orientation of these faults and dykes is not uniform, which indicates a complex tectonic process in the region. All

these tectonic features suggest extension tectonics caused by upwelling of hot mantel material beneath the Yemen region. Figure (17) shows the evaluated compiled solution for general stress field trend for the study region deduced from the analysis of focal mechanism solutions.

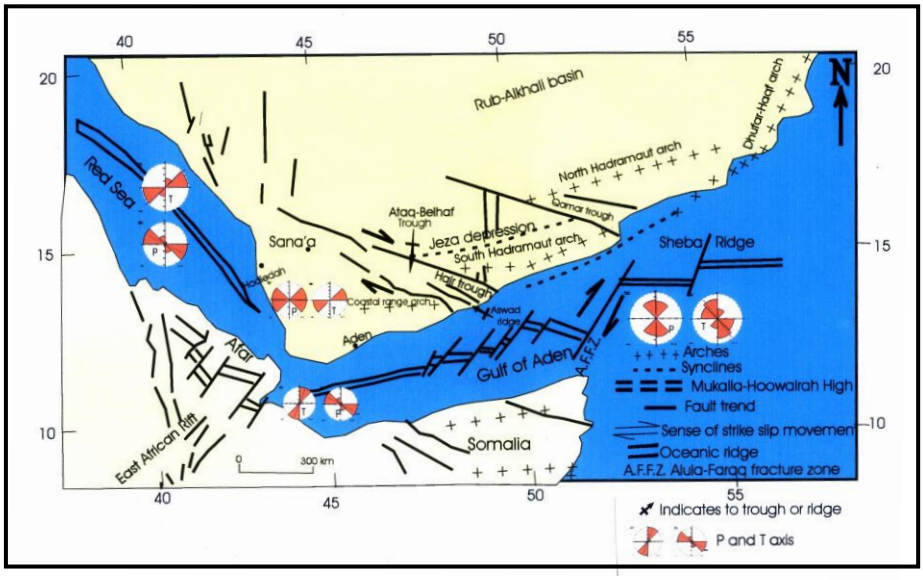

Fig. (17): Evaluated compiled solutions for the general stress field of the southern Red Sea and Yemeni borders deduce from focal mechanism analysis.

E) GPS data Analysis

As we have mentioned before in section (2.1), we used Bernese Ver. 4.2 software (2001) following all constraints and best fetting and consedring the International Rreference Frame and including the important IGS stations for controlling the work, figures (18-20) show the time series for some of these anchor sites . Considering the previous studies, McCluski et al. (2003) deduced the relative motion of Africa plate versus Eurasia plate to be as westward motion and slower convergence in the Mediterranean. That study had been done by collaborative work between MIT and "NRIAG, Helwan", figure (21). We have used here Matrouh station (MATR) in the western north of Egypt to be within the chosen points of the GPS geodetic network

(Yemen-Egypt) and we added another point in the western desert at Kharga (KHRG), review figure (1). Our output results for Matrouh is convenient with that resulted by McCluksy et al, 2003 which asserts the reality of the steady rate motion of the African plate even extracted from the seismological or the GPS data analysis. We have concentrated on the seismological data in the northern Mediterranean Sea to compensate the lack of GPS stations.

The analysis of these focal mechanism solutions are compared with the general trends of the movements deduced from the geodetic analysis and are compliant to a great extent with that deduced from the geodetic data analysis asserting the general trends of the resulted extensional and compressional forces and also the general trend of the fault system. Figure (22) shows the displacement vector deduced from the geodetic GPS data analysis. These are the relative displacements as the final solution in the ITRF 2000 reference frame using Bernese 4.2. Table (4) presents the results of the whole used stations and its coordinates.

Table (4): The whole used stations and its precise coordinates resulted from Bernese V. 4.2 Software.

Station Name	X (M)	Y (M)	Z (M)
ADEN (Asia)	4395393.0338	4401520.1786	1405159.6320
AMMN 22201M001 (Asia)	4386124.5329	3172638.1206	3363685.1977
BAHR 24901M002 (Asia)	3633908.9516	4425275.4972	2799861.3548
DAHA (Asia)	4623441.3966	3174030.6311	3028186.0732
HODE (Asia)	4514928.9872	4203438.0778	1615446.4213
HURG (Africa)	4713701.0127	3159396.8280	2902338.3516
IISC 22306M001 (Asia)	1337937.1312	6070315.4090	1427876.3726
KRGA (Africa)	4918638.5311	2923071.5524	2809674.4495
MALI 33201M001B (Africa)	4865366.4203	4110737.4754	-331121.6483
MATE 12734M008 (Europe)	4641949.6062	1393045.3734	4133287.4132
MKLA (Asia)	4049124.6761	4664309.0865	1585127.2400
MTRH (Africa)	4847936.8523	2494798.5872	3298699.8297
NKLG 32809M002 (Africa)	6287385.8013	1071574.4590	39132.839900
RAMO 20703S001 (Asia)	4514721.9460	3133507.7718	3228024.5941
SANA (Asia)	412796.86010	4289811.5371	1677895.8452
SYON (Asia)	4043087.1904	4614079.5147	1741301.7812
UNIV (Asia)	4896745.2284	3164031.4253	2578555.1427
WTZR 14201M010 (Europe)	4075580.6330	931853.71700	4801568.0828

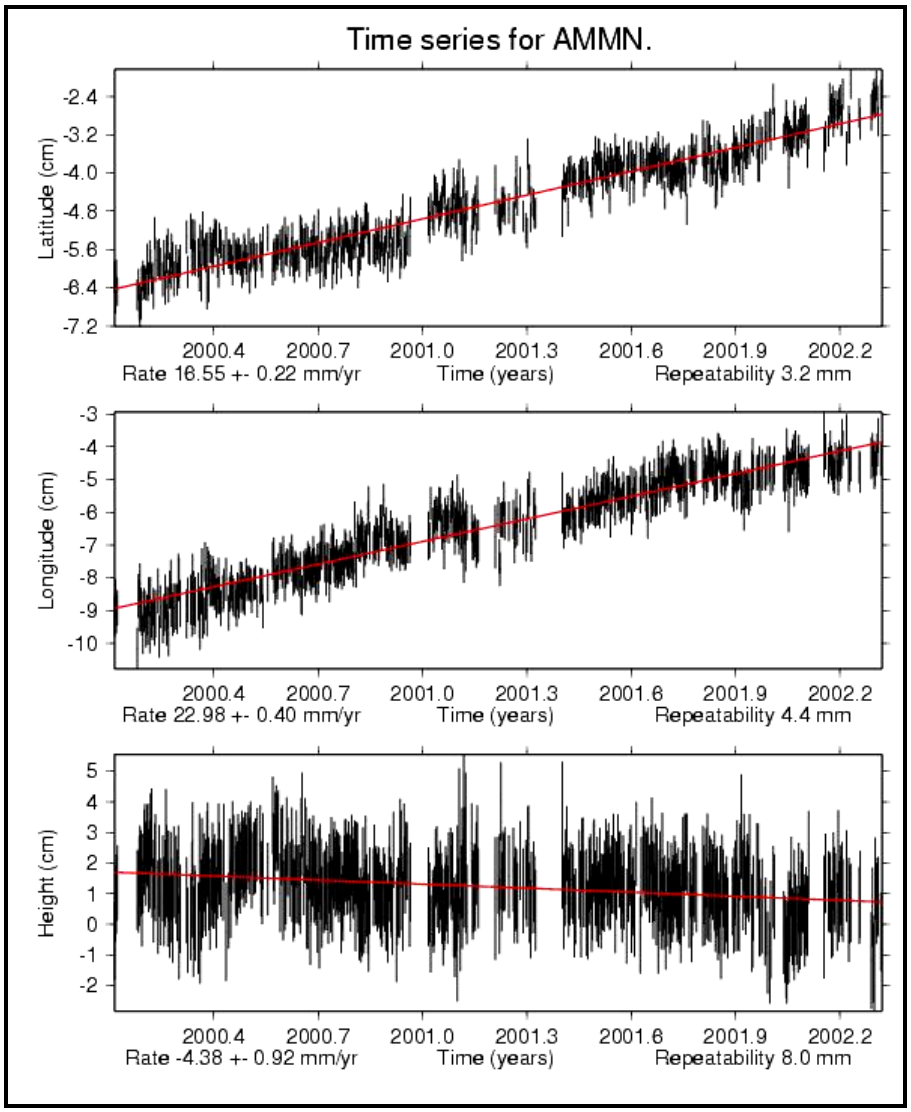

Fig. (18): Time Series for IGS Station Amman, Jordan (AMMN).

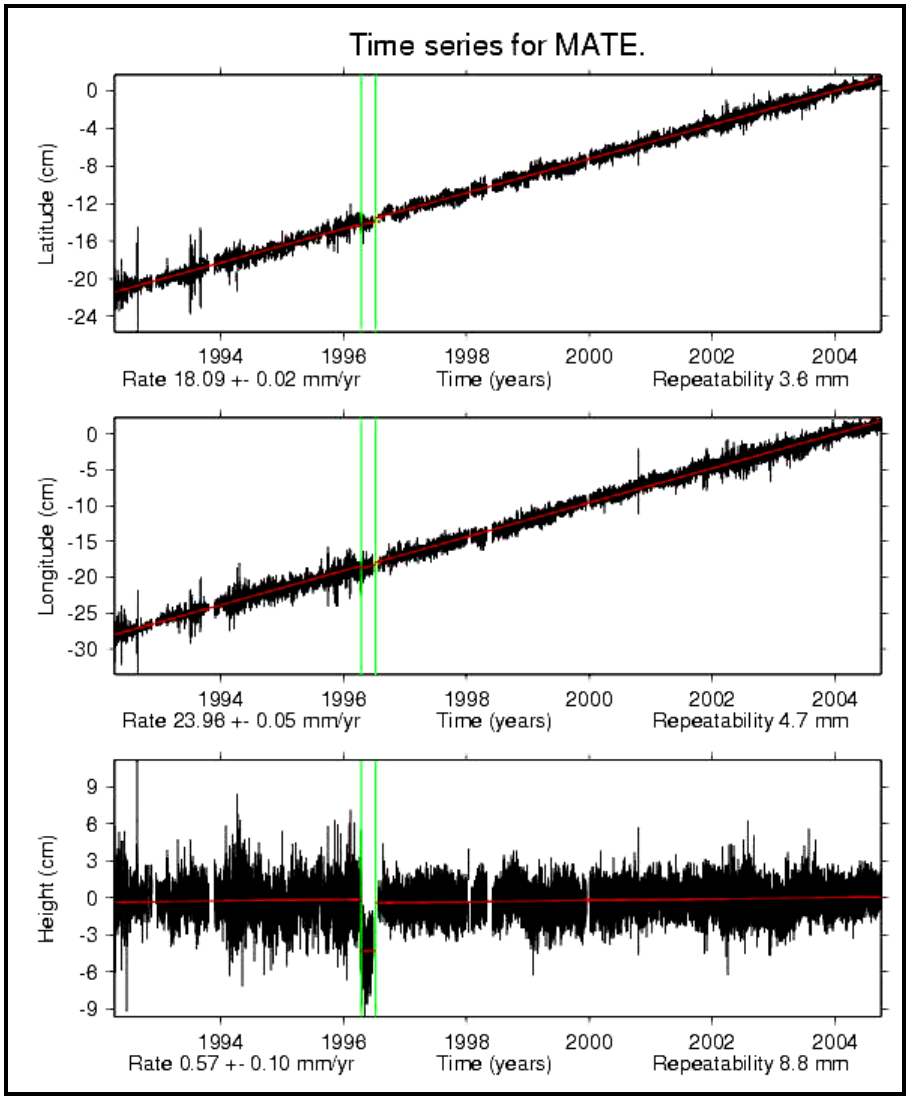

Fig. (19): Time Series for IGS Station Matera, Italy (MATE)

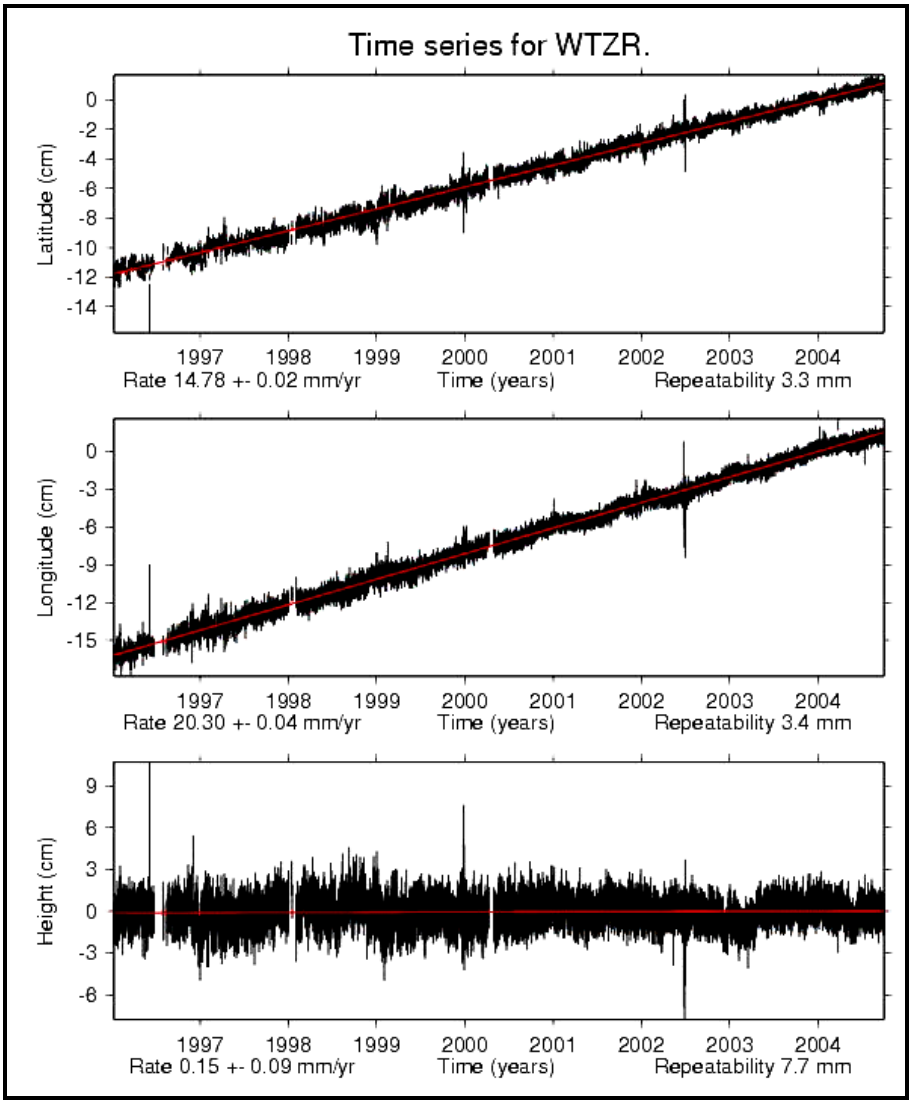

Fig. (20): Time Series for IGS Station Wettzell, Germany (WTZR)

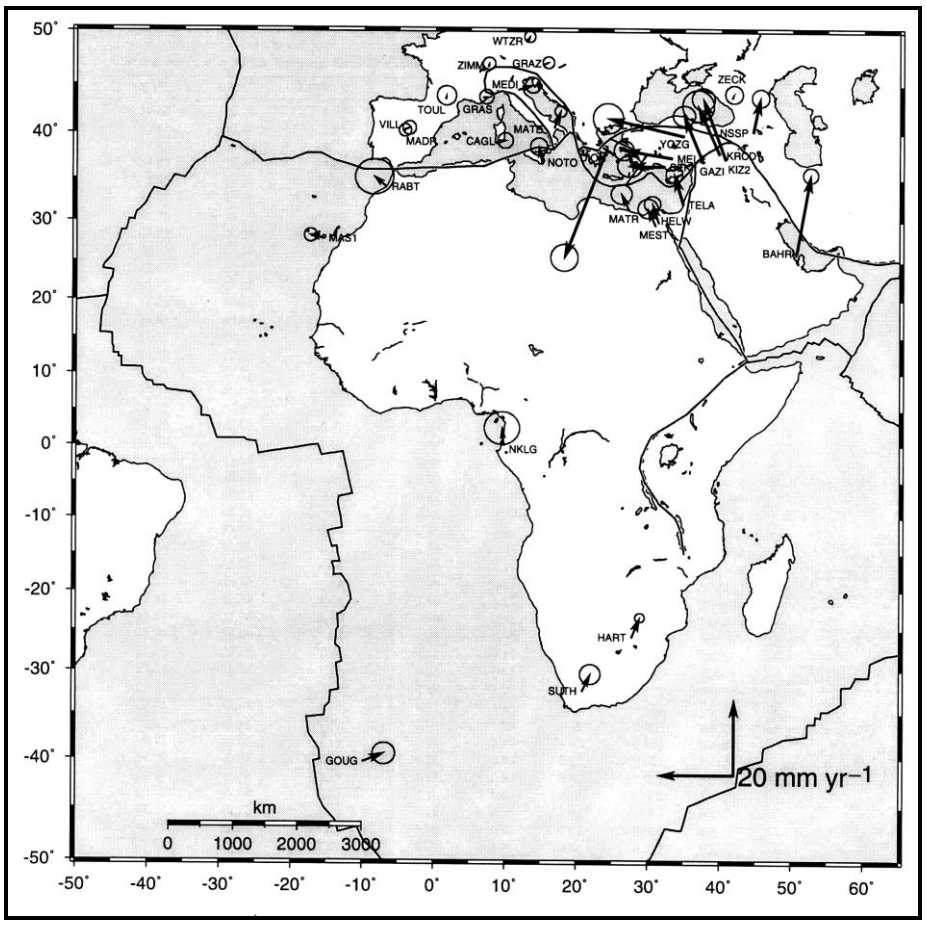

Fig. (21): Shows the chosen Station Matrouh (MATR) and its convenient velocity compared with that of our Egypt-Yemen GPS geodetic Network (After McClusky et al, 2003).

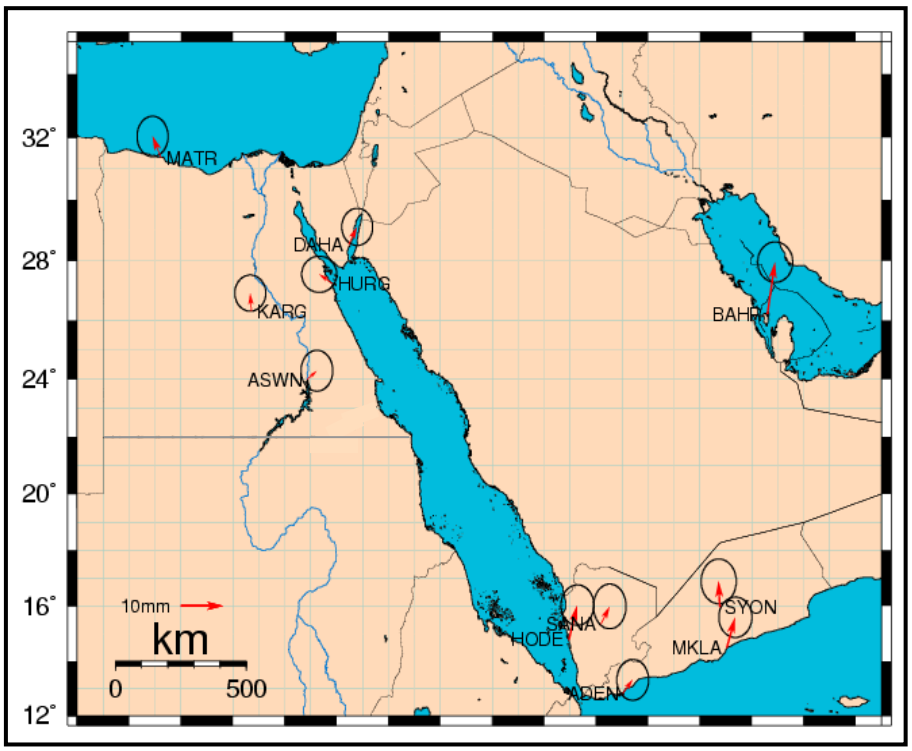

Fig. (22): Shows the general trend of displacements from 2000 to 2003.

Discussion and Conclusions

The implications of deformation, stress, and earthquake activities in the study area are accomplished through the combined solutions from both GPS and seismological data processing. Beginning of the North East African Margin the seismic activity is clearly shown along the northeastern part of Libya (Cyrenaica) which represent the closest area to the subduction process beneath Hellenic arc. Few larger events are located along the Egyptian coastal shelf. The focal mechanisms of larger events along this margin reflect a transition from a tensional stress to the south of the continental shelf to compressional stress to the south of the subduction zone.

The spatial distribution of the earthquake hypocenters (60<h<300 km) on the Hellenic arc indicates that, the subduction of the African plate under the Eurasian plate took place at an angle of about 30° and reaches a maximum depth of about 200 km. The focal mechanisms of shallower earthquakes occurred in the convex side of Hellenic arc show a pure reverse faults and reverse faults with strike slip components. The main trend of P-axis is in SW-NE direction. The trend of T-axis for these events takes the same direction of the dipping slab in western Hellenic arc and rotates to become in NW-SE direction in eastern Hellenic arc. The dominant focal mechanisms of the concave side of the arc are normal faulting which is related to the extensional stress field due to the back arc activity behind the arc. The subduction zone in central Cyprus dips to the NNW with an angle about 25°-30° similar to the Hellenic arc. Rotstein and Ben-Avraham (1985) interpreted the deep seismicity in the Gulf of Anatolia to an earlier subduction, which was active prior to the collision of the Anaximander block and continues to be active today. The direction of the P-axis is NW-SE, which is perpendicular to the arc in its eastern and central parts, but oblique to its western part. The two nodal planes are trending NNW- SSE and NE-SW. The stress tensor analysis for the Cyprian Arc earthquakes indicates to NW-SE trending P-axis. Thus, spatial variations in rate and orientation of the Near East Mediterranean, opening of the Red Sea and African Rift against the rigid motions of the adjacent section of the Arabian plates were detected. The aim of study is concentrated to assert the ongoing results of the study region not to be as specific or independent one. The results of GPS Analysis assert the creeping of Africa versus Europe which observed within the period of investigation from 2000 to 2003 to reach about 4.7 mm/year.

In the Aqaba-Levant Transform fault the activity is trending NNE along the main fault of the Gulf and changed toward the north until Taurus. The activity is diffused in some places due to the intersection of transverse faults with the NNE main trend. From previous focal mechanism solutions along this trend the main trend of T-axis is in N51°E and for P-axis is N65°W. The focal mechanism solutions along

this trend reflect strike slip faults predominantly with normal components. Few events on the eastern side of the Aqaba Gulf. The stress tensor inversion along the Aqaba Gulf gave stress axes σ_1, σ_2 and σ_3 trending azimuth/plunge 333/27, 114/56 and 233/18. The overall deformation of the Arabian-Anatolian boundary seems to separate into two components; a left lateral shear which is absorbed on ENE-striking faults and an NW thrusting on either steep or shallow dipping planes.

To the Southern Red Sea and Yemen territories the seismicity seems to be well correlated with the GPS data in the area. The focal mechanism solutions of the events located in the southern Red Sea suggest pure normal faulting mechanism NNE-SSW trending tension axis along the EAR spreading system indicates typical normal faulting mechanism for most parts with an average tension axis oriented NE-SW reflecting a continental divergent plate boundary. The average direction of the tension axis in the Gulf of Aden is NNE-SSW. such a mechanism reflects a westward extension of the transform fault system and extensional mechanism existing in the Gulf of Aden. The seismic activity along the Sheba Ridge zone is aligned conformably along the main rift axis nearly NWW-SEE. The activity also shows that the rift axis have been transformed by some NE-SW right central strike slip faults. Along the southern part of the Red Sea it is shown two types of faults. The first one from the south indicates normal faulting with large strike-slip components. These solutions have two planes trending NE-SE and NE-SW. The second solution along the southern Red Sea reflects pure normal faulting trending parallel to the Red Sea direction (NW-SE). The general trend of stresses have been evaluated from both the compiled stress field map and the final trend displacement extracted from the GPS data analysis denote to the dominant extensional forces southern of Red Sea and southern borders of Yemen. Some inconsistencies were appeared between GPS relative displacements and seismicity referring to the complex deformation patterns of this region. The spreading velocities parallel to the fracture zone which trends N 35º ranging from 0.9 cm/year in the west to 1.2 cm/year in the east and to reach 2 cm in Bahrain station. These

velocities show impressive agreement with the epicentral distribution, trending west and joining the African rift zone.

The proposed GPS observations are to use an integrated GPS strategy to determine present-day horizontal motions associated with ongoing tectonic trending in the Near East Mediterranean, northern, central, southern Red Sea till the Yemeni borders; to assert the seismological data analysis. The lack of GPS stations at the costal line of North Egypt were compensated with the extensive seismological data analysis and showed the general trends of stresses and discussed within the previous sections. The efforts must be continued through a strong cooperation between the whole institutions in the study region for evaluating the implications of these temporal changes in plate motions. These broader studies will provide much improved constraints on Africa (Nubia)-Arabia and Africa-Eurasia relative motion and will allow us to determine deformation associated with active rifting. In spite of the greater task of that plan and its ultimate objective, we are optimistic to continue to evaluate the geodynamics of this region of interest.

Acknowledgements

We would like to express my deepest thanks and gratitude to, Prof. Dr. Matthias Becker and all colleagues in the Institute of Geodesy, University of the Bundeswehr, Munich for the useful suggestions, to the group of IGS GPS Data Centers. Also, gratitude is extended to the board of Generic Mapping Tools (GMT) Software (Wessel et al.).

References

- **Alaydros, A.A., (2003):** Seismicity, Tectonics and Crustal Deformation in Red Sea Region; Ph.D. Thesis, Dept. of Geology, Banha Faculty of Science, Zagazig University, Egypt.
- **Abou Elenean, K., (1993):** Seismotectonics of the Mediterranean region north of Egypt and Libya; M.Sc. thesis, pp. 198, Faculty of Science, Mansoura University, Egypt.

- **Abou Elenean, K.M., (1997):** Seismotectonics of Egypt in relation to the Mediterranean and Red seas tectonics. Ph. D. thesis, Fac. Sc. Ain Shams Univ., pp. 200.
- **Ambraseys, N., (1978):** Middle East; A reappraisal of the seismicity; J. Eng. Geol., 11, pp. 19-32.
- **Ben-Avraham, Z., Nur, A. and Cello, G., (1987):** Active transcurrent fault system along the north African passive margin; Tectonophys. V. 141, pp.294-260.
- **Bosworth, W. and Taviani, M., (1996):** Late Quaternary orientation of stress field and extension direction in the southern Gulf of Suez, Egypt: Evidence from uplifted coral terraces
- **Buyukasikoglu, S., (1980):** Eurasian-African plate boundary in southern Turkey and eastern Mediterranean, in Proceeding of the 7th World Conference on Earthquake Engineering, Geo-Science Aspects, Part 1, Vol. 1, 209-212.
- **Korrat, I.M., Ibrahim, E.M., Shrief, R.M. and Abou Elenean, K.M., (1996):** Earthquake mechanisms in the Eastern Mediterranean region and their tectonic implications. Bull. IISEE, Vol. 30, 29-44.
- **McCusky, S., Reilinger. R., Mahmoud, S., Ben Sari, D. and Tealeb, A., (2003):** "GPS Constraint on Africa (Nubia) and Arabia Plate Motions" Journal of Geophysics 155, 126-138.
- **Matthias, B. (2002):** Personal Contact."universität der bundeswehr München Fkultaet fuer Bauingenieur und Vermessungen -Institut fuer geodaesie.
- **Matthias, B.; Carine, B. and Rui F. (On Behalf of the Wegener Diorectory Board) (2002):** "Processing And Submission Guidelines For GPS Solutions to be Integrated to A Wegener Data Base"universität der bundeswehr München Fakultaet fuer Bauingenieur und Vermessungen - Institut fuer geodaesie.
- **McKenzie, D., (1970):** Plate tectonics of the Mediterranean region; Nature, 326, pp. 239-243.
- **McKenzie, D., (1972):** Active tectonics in the Mediterranean region; Geophys., J. R. Astron. Soc., 30, pp. 109-185.
- **McKenzie, D., (1978):** Active tectonics of the Alpine- Himalayan belt: The Aegean and surrounding regions; Geophys. J. R. Astron. Soc., 55, pp. 217-254.
- **Papadopoulos, G.A., Kondopoulou, D.P., Leventakis, G.A. and Pavlides, S.B., 1986:** Seismotectonics of the Aegean Region, Tectonophys. V.124, 67-84.

- **Papazachos, B. and Comninakis, P., (1978):** Deep structure and tectonics of the eastern.
- **Pedone et al., (1992):** Mesoscopic fault arrays and borehole breakouts. Tectonics, 15, 4,791-802.
- **Bernese GPS Software Operation Manual, (2001):** Astronomical Institute University Of Berne, Switzerland. version 4.2
- **Rotstein, Y. and Ben-Avraham, Z., 1985:** Accretion processes at subduction zones in the eastern Mediterranean; Tectonophys. V. 112, pp. 551-561.
- **Said, R., (1990):** "The Geology Of Egypt", A. A. Balkema, Rptterdam, Brookfield.
- **Salamon, A., Avraham, H., Garfunkel, Z. and Ron, H., 2003:** Seismotectonics of Sinai subplate-Eastern Mediterranean Region, Geophys. J. Int. 155, 149-173.
- **Schneider, D., (1982):** "Complex Crustal Strain Approximation", University Of New Brunswick, Fredericton, N. B. And Institute Of Geodesy And Photogrammetry, Swiss Federal, Institute Of Technology, Zürich. NPPA Ministry of Electricity, Egypt.
- **Sofratome Group, (1984):** Regional Geology, tectonics and seismology, Chapter 3,21-32
- **Trimble, N.L., (1997):** "TRIMNET Plus Software's User Manual", Trimble Navigation Limited, Sunnyvale, U.S.A. Angerman D., J. Klotz, C. Reigber, Space-geodetic estimate of the Nazca-South America Euler vector, Earth Planet. Sci. Lett., 171, 329-334, 1999.

* * *